

Bexarotene Does Not Clear Amyloid Beta Plaques but Delays Fibril Growth: Molecular Mechanisms

Pham Dinh Quoc Huy,^{†,‡,¶} Nguyen Quoc Thai,^{§,||,¶} Zuzana Bednarikova,[±] Le Huu Phuc,^{⊥,¶} Huynh Quang Linh,^{||} Zuzana Gazova,^{*±} and Mai Suan Li^{*,†,¶}

[†]Institute of Physics, Polish Academy of Sciences, Al. Lotnikow 32/46, 02-668 Warsaw, Poland

[‡]Institute for Computational Science and Technology, Quang Trung Software City, Tan Chanh Hiep Ward, District 12, Ho Chi Minh City, Vietnam

[§]Division of Theoretical Physics, Dong Thap University, 783 Pham Huu Lau Street, Ward 6, Cao Lanh City, Dong Thap, Vietnam

^{||}Biomedical Engineering Department, University of Technology, VNU HCM 268 Ly Thuong Kiet Street, District 10, Ho Chi Minh City, Vietnam

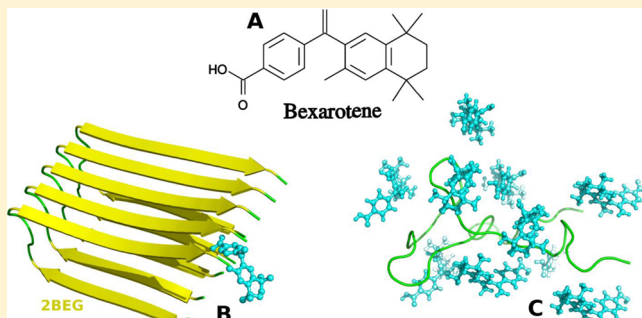
[±]Department of Theoretical Physics, University of Natural Sciences, VNU, 227 Nguyen Van Cu, District 5, Ho Chi Minh City, Vietnam

[⊥]Department of Biophysics Institute of Experimental Physics, Slovak Academy of Sciences, Watsonova 47, 040 01 Kosice, Slovakia

S Supporting Information

ABSTRACT: In 2012, it was reported that anticancer drug bexarotene reduced amyloid plaque and improved mental functioning in a small sample of mice engineered to exhibit Alzheimer's like symptoms. It has been suggested that bexarotene stimulates expression of apolipoprotein E (ApoE) leading to intracellular clearance of amyloid beta ($A\beta$). However, the effect of bexarotene on clearance of plaques has not been seen in some mouse models. Two interesting questions include whether bexarotene can destroy $A\beta$ fibrils via direct interaction with them and how this compound impacts the lag phase in the fibril growth process. By the Thioflavin T fluorescence assay and atomic force microscopy, we have shown that bexarotene prolongs the lag phase, but it does not degrade $A\beta$ fibrils. The impotence of bexarotene in destroying fibrils means that this compound is weakly bound to $A\beta$. On the other hand, the weak binding would prevent bexarotene from prolonging the lag phase. Thus, our two main in vitro observations seem to contradict each other. In order to settle this problem at the atomic level, we have performed all-atom molecular dynamics simulations in explicit water. We have demonstrated that bexarotene is not capable to reduce amyloid deposits due to weak binding to $A\beta$ fibrils. However, it delays the self-assembly through reduction of the β -content of $A\beta$ monomers at high enough ligand concentrations. Bexarotene is the first compound which displays such an unusual behavior. We have also shown that bexarotene has a low binding propensity to $A\beta$ monomer and dimer.

KEYWORDS: Bexarotene, amyloid beta peptide, $A\beta$ fibril, $A\beta$ oligomer, binding free energy



INTRODUCTION

Alzheimer's disease (AD) is one of the most common neurodegenerative diseases, mainly affecting the senior population.¹ Financially, it is very costly and poses a great burden to society. Despite intense research during the last decades, no therapies have passed clinical trials as genetic and molecular mechanisms behind this disease remain largely unclear. The amyloid cascade hypothesis posits that AD is pathologically associated with progressive extracellular accumulation of amyloid deposits which mainly consist of amyloid beta ($A\beta$) peptides of 36–43 amino acids.² They are generated from APP (amyloid precursor protein) which is cut by β - and γ -secretases. The most abundant forms of $A\beta$ peptides are $A\beta_{1-40}$

and $A\beta_{1-42}$ which have 40 and 42 amino acids, respectively. Experimental and simulation data have shown that they are intrinsically disordered in a monomeric state in water environment³ but under specific conditions can aggregate into fibrils consisting of ordered β -sheets.^{4,5} Recent studies suggest that soluble oligomers are more toxic than mature fibrils and cause cell death.^{2,6} Although the question about the presence of oligomers on pathways to fibers remains obscure,

Received: March 23, 2017

Accepted: July 9, 2017

Published: July 9, 2017

one of the promising therapies for AD is to prevent self-assembly of $A\beta$ peptides.^{7,8}

Bexarotene (brand name: Targretin, the 2D structure is given in Figure 1) is an anticancer agent which is used as a treatment

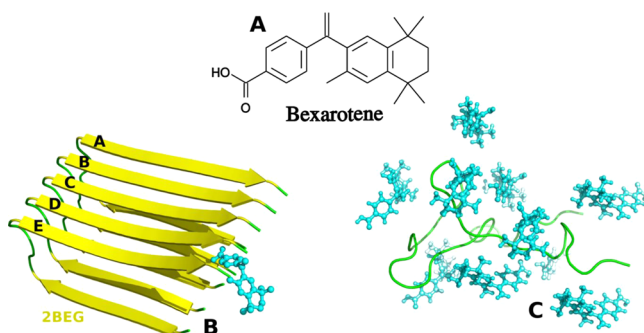


Figure 1. Two-dimensional structure of bexarotene (A), the PDB 5A β ₁₇₋₄₂ (2BEG) with bexarotene in the best docking mode (B), and monomer A β ₁₋₄₂ with 10 bexarotenes around (C).

for cutaneous T cell lymphoma.⁹ Recently, Cramer et al.¹⁰ have reported that bexarotene shows astonishing efficacy in mice models of AD, reducing $A\beta$ plaques by about 50% within just 72 h. The authors have reasoned their finding as follows. The polymorphic gene encoding APOE (apolipoprotein E) has three allelic variants, which include ApoE2, ApoE3, and ApoE4 in humans. The latter allele is considerably overexpressed in AD patients, occurring in 40–65% of affected people. The ApoE expression is regulated via action of nuclear receptors PPAR- γ (peroxisome proliferator-activated receptor γ) and retinoid X receptors. The bexarotene binding to these receptors enhances ApoE association with lipoproteins leading to formation of APOE-associated lipoprotein particles that can interact with soluble $A\beta$ to stimulate its clearance from the brain.¹¹

After the publication by Cramer et al., several groups around the world have made attempts to repeat their *in vivo* experiment, but contradictory results were reported. Namely, the strong $A\beta$ clearance was not reproducible in some mouse models but not in all of them. One of the mechanisms for $A\beta$ clearance was based on data obtained in murine models of AD that nuclear receptor agonists (GW0742 and bexarotene) elevate Axl and MerTK expression on plaque-associated macrophages leading to reduction in plaque burden.¹² Marinari

and collaborators reported¹³ that a 3.5 month old SXFAD mice treated with bexarotene improved cognition correlated with reduced plaque burden and suppression of inflammatory gene expression.

Fitz et al. demonstrated¹⁴ that bexarotene substantially improved cognitive deficits in APP/PS1 Δ E9 mice, but they failed to confirm its effect on amyloid plaques in hippocampus and cortex. They hypothesized that bexarotene displays its effect on memory via a non- $A\beta$ related pathway. The effect of bexarotene in clearance of $A\beta$ deposits including oligomers and plaques was not also observed in the APP/PS1 mice.¹⁵ Tessier and collaborators¹⁶ were not able to reproduce data of Cramer et al.¹¹ either in beagle dogs or mice. Interestingly, bexarotene reduced soluble $A\beta$ 40 levels in one of the mouse models, and the drug had no effect on plaque burden in three strains which exhibit $A\beta$ amyloidosis.¹⁷

Ghosal et al. have shown that although bexarotene elevated CSF apoE by about 25%, it had no impact on $A\beta$ metabolism.¹⁸ This may be caused by low nM levels in CSF despite high 1–2 μ M levels found in plasma due to its oral administration. Using several transgenic mouse models of AD and tests on rats, it was shown that bexarotene administration had no effect on $A\beta$ deposits in cerebral cortex and on $A\beta$ -induced cognitive decline.¹⁹

Taken together, it remains unclear whether bexarotene can directly destroy fibrils and how it influences the fibril growth process, in particular, the lag phase. From the theoretical point of view the role of bexarotene in AD pathways remains also obscure.

In order to probe the direct interaction of bexarotene with $A\beta$ fibrils (i.e., to exclude pathways via APOE), we have performed *in vitro* experiments using the Thioflavin T fluorescence assay and atomic force microscopy technique. We have shown that bexarotene does not spoil fibril patterns implying the weak interaction between them. However, our *in vitro* experiment shows that this compound prolongs the lag phase, suggesting that the interaction of bexarotene with $A\beta$ is not weak. Thus, this effect seems to conflict with the fact that bexarotene cannot clear fibrils.

To resolve this dilemma, we have carried out the all-atom molecular dynamics (MD) simulations for several $A\beta$ -bexarotene complexes. Combining the docking and molecular mechanics-Poisson–Boltzmann surface area (MM-PBSA)²⁰ method we have shown that bexarotene is weakly bound to

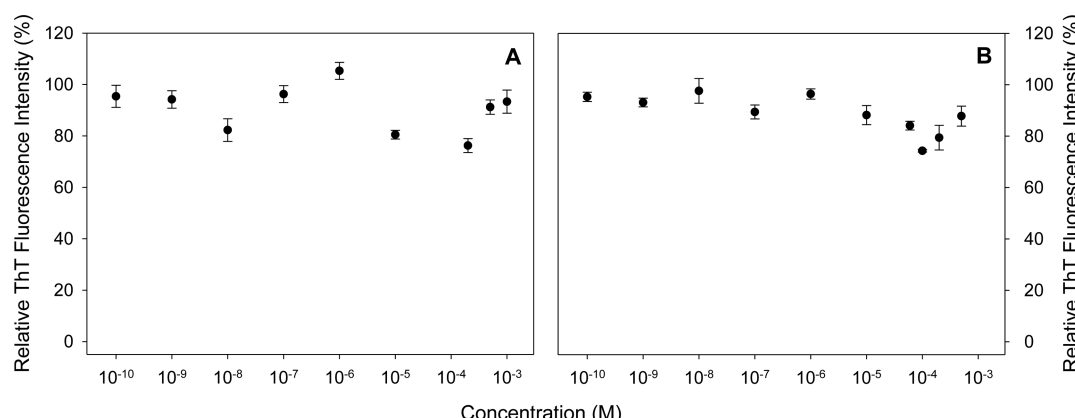


Figure 2. Concentration dependence of the effect of bexarotene on $A\beta_{1-42}$ peptide amyloid aggregation detected using ThT assay. The effect of bexarotene on $A\beta_{1-42}$ fibrillization (A) and on $A\beta_{1-42}$ fibrils (B).

$\text{A}\beta$ fibrils, consistent with our in vitro result on its impotency in clearance of fibrils. By the replica exchange MD (REMD) simulation, we demonstrated that at high enough bexarotene concentrations the β -content of $\text{A}\beta_{1-42}$ monomer is reduced leading to prolongation of the lag phase. Thus, our study has revealed the molecular mechanisms underlying impact of bexarotene on $\text{A}\beta$ fibril growth and stability.

RESULTS AND DISCUSSION

Antiamyloid Activity of Bexarotene. The antiamyloid properties of bexarotene were observed using Thioflavin T assay. The ability of bexarotene to affect $\text{A}\beta_{1-42}$ peptide amyloid aggregation as well as amyloid fibrils was studied within concentration range of compound from 100 pM up to 1 mM and 10 μM $\text{A}\beta_{1-42}$ peptide concentration. The obtained data are presented in Figure 2A (effect on formation of amyloid aggregates) and Figure 2B (effect on amyloid fibrils), where the fluorescence intensities were normalized to the fluorescence signal of $\text{A}\beta_{1-42}$ amyloid aggregates alone, 100%. These data clearly show that bexarotene within the studied concentration range has no significant effect on fibrillization of $\text{A}\beta_{1-42}$ peptide (Figure 2A) as the fluorescence intensities of the samples are comparable to untreated $\text{A}\beta_{1-42}$ peptide aggregation ($\sim 80-100\%$). Moreover, bexarotene also was not able to destroy formed $\text{A}\beta_{1-42}$ fibrils (Figure 2B) as there was no decrease of fluorescence intensities detected for $\text{A}\beta_{1-42}$ fibrils treated with increasing concentration of bexarotene.

Atomic Force Microscopy. Atomic force microscopy (AFM) was used to confirm and visualize the effect of bexarotene on $\text{A}\beta_{1-42}$ peptide fibrillization and $\text{A}\beta_{1-42}$ amyloid fibrils (Figure 3). $\text{A}\beta_{1-42}$ amyloid fibrils have typical

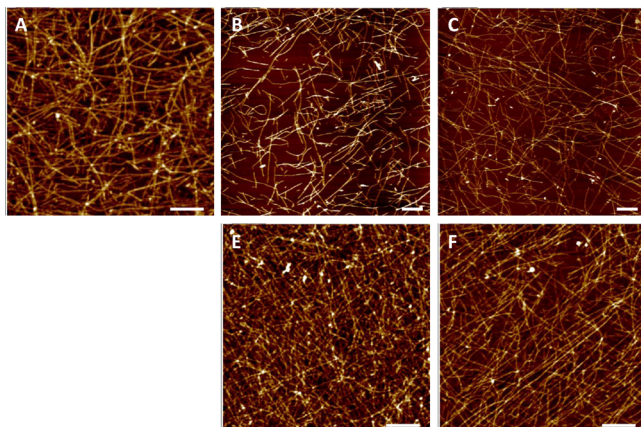


Figure 3. AFM images of 10 μM $\text{A}\beta_{42}$ fibrils formed alone (A) and in the presence of 1 mM (B) and 100 pM (C) bexarotene. $\text{A}\beta_{42}$ fibrils after treatment with 100 μM (E) and 10 μM (F) bexarotene. Bars represent 1 μm .

morphology—unbranched fibrillar aggregates, several μm long (Figure 3A). The presence of 10 μM and 100 μM bexarotene during the process of fibrils formation does not lead to the reduction of the amount of $\text{A}\beta_{1-42}$ fibrillar aggregates as the AFM images (Figure 3B,C) are similar to the image of the $\text{A}\beta_{1-42}$ untreated fibrillization (Figure 3A), confirming the very weak ability of bexarotene to affect $\text{A}\beta_{1-42}$ fibrillization. Similarly, there was no changes in the morphology and amount of $\text{A}\beta_{1-42}$ fibrils after treatment with 100 pM or 1 mM bexarotene (Figure 3E,F).

Kinetic Study of Inhibitory Effect of Bexarotene. We are well aware of the work of Habchi et al.,²¹ who have shown that bexarotene is able to prolong the lag phase of $\text{A}\beta_{1-42}$ peptide fibrillization due to inhibition of secondary nucleation. However, they still observed formation of fibrillar aggregates, which is in agreement with our results. We aimed to determine if in our condition (higher concentration of $\text{A}\beta_{1-42}$ peptide, acidic pH) bexarotene is able to influence one of the steps of fibrillization. Therefore, the kinetics of the fibrils formation in the presence of increasing concentration of bexarotene was studied using Thioflavin T fluorescence assay. The kinetics profiles of the $\text{A}\beta_{1-42}$ peptide fibrillization in the presence of 10, 50, and 100 μM bexarotene are shown in Figure 4. The data

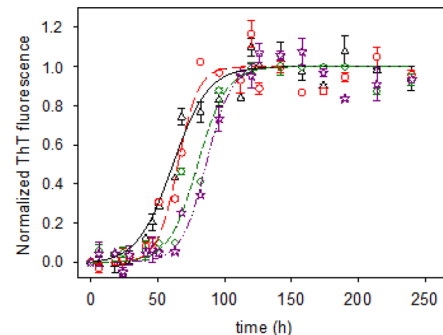


Figure 4. Kinetic profiles of 10 μM $\text{A}\beta_{1-42}$ fibrillization alone (black triangles) and in the presence of bexarotene monitored by ThT fluorescence assay. The bexarotene concentrations are 10 μM (red circles), 50 μM (green diamonds), and 100 μM (purple stars). The obtained data were normalized to the average steady-state fluorescence intensity values detected for each growth curve (taken as 1). The error bars represent the standard deviation of three independent samples. The curves were fitted using nonlinear least-squares method.

were normalized to the average of steady-state fluorescence intensities of untreated $\text{A}\beta_{1-42}$ fibrils formation (taken as 1). The growth curve of $\text{A}\beta_{1-42}$ fibrils formation (black triangles) follows nucleation-polymerization kinetics with typical sigmoidal profile with lag phase lasting about 25 h followed by elongation phase with steep increase of fluorescence intensities. The process is finished after 100 h as the fluorescence intensities reached steady-state values.

The presence of bexarotene changed the time of lag phase when compared to the $\text{A}\beta_{1-42}$ peptide fibrils formation alone. In the case of 10 μM bexarotene concentration, the lag phase lasted about 47 h (red circles). Further increase of bexarotene concentration led to an even longer lag phase, namely, about 55 h for 50 μM (green diamonds) and 65 h for 100 μM bexarotene concentrations (purple stars).

The obtained results indicate that bexarotene can prolong the lag phase and thus delays formation of nuclei, oligomers, and subsequent formation of fibrils.

Docking Results. The structure obtained in the best docking mode for bexarotene in complex with 5 $\text{A}\beta_{17-42}$ is shown in Figure 1B. Because bexarotene contains only two oxygen atoms the HB network is so poor, that there is no HB between bexarotene and 5 $\text{A}\beta_{17-42}$ (Figure S1 in SI). The weak binding affinity to fibril ($\Delta E_{\text{bind}} = -7 \text{ kcal/mol}$) is consistent with the absence of HBs and this will be also confirmed by MD simulation.

Bexarotene Does Not Destroy $\text{A}\beta_{42}$ Fibril Due to Low Binding Affinity. Low Binding Affinity of Bexarotene to

A β 42 Fibril. To estimate ΔG_{bind} of bexarotene to $5A\beta_{17-42}$ we have performed four independent MD runs starting from the same initial configuration shown in Figure 1B but with different seed numbers. Because the $A\beta$ 42 fibril does not have a well-defined binding site to reach equilibrium in all trajectories we have extended MD simulations up 200 ns (Figure S2). The equilibration time, τ_{eq} , is defined as the time when the interaction energy and RMSD saturate. Clearly for the $5A\beta_{17-42}$ -bexarotene complex, τ_{eq} is sensitive to MD runs ranging from about 40 to 160 ns.

Using eq 1 and snapshots collected at equilibrium (i.e., after the arrow in Figure S2), we have calculated ΔG_{bind} for each MD trajectory (Table S1 in SI). The vdW interaction is superior over the electrostatic interaction in directing bexarotene to bind to $5A\beta_{17-42}$. The binding free energy depends on trajectories, but overall it remains low in all runs, and especially, in the fourth run it becomes positive (Table S1).

The low binding affinity ($\Delta G_{\text{bind}} \approx -0.7$ kcal/mol) to $A\beta$ fibril supports our in vitro results (Figure 2B, Figure 3) that bexarotene is unable to clear amyloid fibrils or reverse the aggregation process. This conclusion is further supported by our simulations presented below.

Residues Leu17 (chain A), Leu17, and Phe19 (chain B); Leu17, Gly37, and Val40 (chain C); Phe19, Val40, Ile41, and Ala42 (chain D); and Leu17, Phe19, Val40, Ile41, and Ala42 (chain E) significantly contribute to the vdW interaction with bexarotene (Figure S3). In the case of electrostatics interaction residues Leu17 (chain C), Leu17, Val36 and Ala42 (chain D), and Leu17 (chain E) are crucial. Residues Ile41 and Ala42 of chain E reduce the binding propensity through repulsive interaction with bexarotene (Figure S3). Overall, chains C, D, and E are dominating in stabilization of bexarotene in complex with $5A\beta_{17-42}$. This is also in the line with the docking result that bexarotene is located near these chains in the best docking mode (Figure 1). The C-terminal is decisive in bexarotene binding toward 2BEG fibril.

Is the Binding Affinity of Bexarotene to A β 42 Fibrils Sensitive to Fibril Targets? In the previous section, we have shown that the binding of bexarotene to $5A\beta_{17-42}$ is weak. Because of polymorphism of fibril structures, a natural question emerges is whether the binding affinity depends on the structure of target. To answer this question, we have performed additional simulations for truncated $12A\beta_{11-42}$ (PDB ID: 2MXU²²) and $10A\beta_{11-42}$ (PDB ID: SKK3²³) and full-size $6A\beta_{1-42}$ (PDB ID: 2NAO²⁴) fibrils. In contrast to $5A\beta_{17-42}$, the chain in the fibril state of these targets has the S-shape which is believed to be more reasonable than the U-shape.²⁵ Next, we will present results on the binding affinity of bexarotene to these three targets obtained by the docking and MD simulation.

1. $12A\beta_{11-42}$ (2MXU). For simulation, we retrieved from PDB the structure which has 12 S-shape chains in fibrillar state. Figure S4 in SI shows the best docking mode structure with the binding energy $E_{\text{bind}} = -7.8$ kcal/mol which is lower than that of $5A\beta_{17-42}$. This is probably because bexarotene seats deeper inside 2MXU compared to $5A\beta_{17-42}$. Bexarotene forms two HBs with Gly33 from chain E and one HB with Ile32 from chain F implying that bexarotene prefers to locate in the hydrophobic C-terminal region. The stronger binding affinity of bexarotene to 2MXU compared to 2BEG is associated with different HBs that it forms 3 HBs with 2MXU but none with 2BEG. In addition, bexarotene forms more nonbonded contacts with 2MXU (12 contacts) compared to 2BEG (9 contacts) (Figures S1 and S4).

Using the structure obtained in the best docking mode (Figure S4) as initial configuration, we have performed seven independent MD runs of 200 ns. The complex reaches equilibrium at different times ranging from about 65 to 160 ns (Figure S5). The binding free energy, obtained by using the MM-PBSA method and equilibrium phase snapshots, is given in Table S2 in SI. As in the 2BEG case, the entropy and ΔG_{sur} terms are not so sensitive to MD trajectories. Also, the vdW interaction is dominating over the electrostatic interaction in binding affinity of bexarotene to $12A\beta_{11-42}$. Because $\Delta G_{\text{bind}} \approx -14 \pm 4$ kcal/mol, contrary to the 2BEG case, bexarotene strongly binds to 2MXU, implying the dependence of binding affinity on target structure.

2. $10A\beta_{11-42}$ (5KK3). Because the results on bexarotene binding affinity to 2BEG and 2MXU contradict each other, we have carried out simulation using the $10A\beta_{11-42}$ fibril as target. The rationale for our choice is that the chains in truncated SKK3 have the same length (32 residues) and the S-shape in fibril state as 2MXU. The difference between two targets is only in structures of the fibrillar state (Figures S4 and S6). The PDB structure SKK3 has 18 chains, but to reduce computational cost, we kept only 10 chains. In the best docking mode (Figure S6), we have $E_{\text{bind}} = -7.9$ kcal/mol, which is close to that of 2MXU. Bexarotene forms only one HB with SKK3 (Figure S6), while it has 3 HBs with 2MXU, suggesting that bexarotene binds to SKK3 weaker than to 2MXU. This is also consistent with the poorer nonbonded contacts network of SKK3 (10 contacts) in comparison with 2MXU (12 contacts).

In order to further elaborate the bexarotene binding affinity to SKK3, we computed the binding free energy by the MM-PBSA method. In MD runs 1 and 3, the complex reaches equilibrium at larger time scales than in runs 2 and 4 (Figure S7). Using snapshots recorded after the arrow in Figure S6 and eq 1, we obtained the binding free energy shown in Table S3. Clearly, bexarotene weakly binds to SKK3 having $\Delta G_{\text{bind}} \approx 0.8 \pm 3.0$ kcal/mol. The low binding affinity is mainly caused by the weak vdW interaction.

The results obtained for truncated fibrils are not convincing enough as the binding affinity of bexarotene is weak for two targets (2BEG and SKK3), but it is strong for the 2MXU target motivating us to study the full-length fibril $6A\beta_{1-42}$.

3. $6A\beta_{1-42}$ (2NAO). To model the full length $A\beta_{1-42}$ fibril we used the structure 2NAO²⁴ which has 6 S-shape chains. In the docking lowest energy state (Figure S8) $E_{\text{bind}} = -7.8$ kcal/mol. Clearly, the docking method provides nearly the same binding energy for three targets with S-shape chains including 2MXU and SKK3. In the best docking mode, bexarotene forms 2 HBs and 9 nonbonded contacts with the fibril (Figure S8). The poor HBs and nonbonded contacts networks are indicative of low binding propensity of bexarotene as will be confirmed by the MM-PBSA calculation.

Starting from the structure obtained in the best docking mode (Figure S8), we have performed four independent MD simulations with different seed numbers for generating different velocity fields. The equilibration time for the 2NAO +bexarotene complex varies from about 25 ns (Trajectory 3) to 110 ns (Trajectory 1) (Figure S9 in SI). Shown on Table S4 is the binding free energy estimated at equilibrium by the MM-PBSA method. As in the other cases, the vdW interaction is a driving force for binding of bexarotene to the 2NAO fibril. Because this interaction is remarkably weaker than that of 2MXU (Tables S2 and S4), the binding affinity of bexarotene to $6A\beta_{1-42}$ is low with $\Delta G_{\text{bind}} \approx -0.2 \pm 6.2$ kcal/mol.

Taken together, as expected, the binding affinity is sensitive to fibril targets. However, because 2NAO is a full-length fibril, the low binding affinity obtained for this model is the most relevant for comparison with experiment. Furthermore, for the four studied targets, the strong binding occurs in just one case of 2MXU. Thus, our *in silico* results support the experimental fact that bexarotene does not destroy $\text{A}\beta_{42}$ fibril due to its low binding affinity.

Bexarotene Does Not Destroy $\text{A}\beta_{42}$ Fibrils. The weak binding of bexarotene to $5\text{A}\beta_{17-42}$ fibrils suggests that bexarotene is not involved in direct $\text{A}\beta$ clearance from the brain. To ascertain this directly, we have carried out 200 ns MD simulations to probe stability of $5\text{A}\beta_{17-42}$ fibril in the absence and presence of bexarotene. The PBD structure 2BEG was used as the starting configuration for $5\text{A}\beta_{17-42}$ without bexarotene, and four independent runs were carried out using different random seed numbers. In order to study the influence of bexarotene on the fibril stability, we performed two sets of MD simulation. In the first set, three independent MD runs have been generated starting from the configuration which involves the PDB structure 2BEG with six bexarotene molecules randomly added (Figure 5A). In the second set, the initial

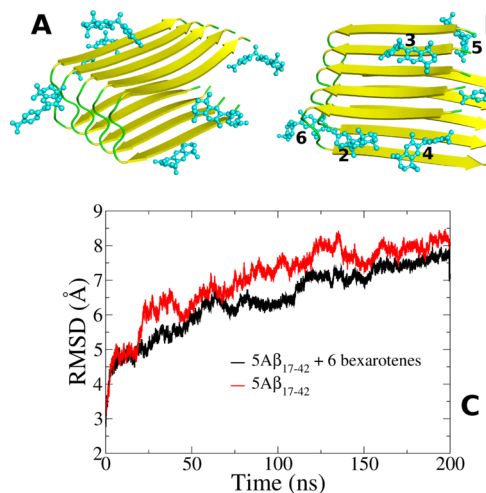


Figure 5. (A) Typical starting configuration for simulation of the fibril stability in the presence of bexarotene. Six bexarotene molecules are randomly placed around $5\text{A}\beta_{17-42}$. (B) The same as in (A) but molecules 1–5 were put in lowest binding energy positions obtained by the docking method, while molecule 6 was randomly added. (C) Time dependence of RMSD for $5\text{A}\beta_{17-42}$ (red) and $5\text{A}\beta_{17-42} + 6$ bexarotenes (black) systems. The results are averaged over four MD trajectories.

structure for MD simulation was generated in such a way that five bexarotene molecules were placed at the five lowest binding energy positions (note that in the 20 best docking modes bexarotene was located in one of these five positions), whereas the sixth bexarotene was randomly added (Figure 5B).

Table 1. Binding Free Energy (kcal/mol) of Bexarotene to $\text{A}\beta_{42}$ Monomer, Dimer, and Protomeric^a

targets	ΔE_{vdw}	ΔE_{ele}	ΔG_{PB}	ΔG_{sur}	$-T\Delta S$	ΔG_{bind}
monomer	-26.5	-7.7	18.4	-2.9	17.0	-1.8
dimer	-18.5	-7.6	14.5	-2.1	14.3	0.6
$5\text{A}\beta_{17-42}$	-30.5 ± 6.1	-7.3 ± 4.0	22.9 ± 4.4	3.4 ± 0.4	17.5 ± 1.8	-0.7 ± 5.0

^aResults were obtained by the MM-PBSA method.

Figure S10 in SI shows the time dependence of RMSD for $5\text{A}\beta_{17-42}$ and $5\text{A}\beta_{17-42} + 6$ bexarotenes in 4 MD runs. Both systems reached equilibrium with the RMSD saturation in all trajectories. As expected, the result is sensitive to starting configurations but RMSD remains below 10 Å for both systems. The mean RMSD (Figure 5C), obtained by averaging over four trajectories, also indicates that the presence of six bexarotenes has little impact on the stability of fibril. This is in the line with the low binding affinity revealed by the MM-PBSA method. Thus, the clearance of $\text{A}\beta$ deposits in the brain is not associated with the direct interaction of bexarotene with $\text{A}\beta$ peptides.

Bexarotene Delays the Nucleation through Reduction of the β -Content of Monomer. As shown by our *in vitro* (Figure 4) and *in vivo*²¹ experiments, bexarotene prolongs the lag phase, raising the interesting question as to whether interferes with early events in fibril growth strongly binding to monomers and oligomers. In order to answer this question, we have calculated the binding free energy of bexarotene to monomers and dimers.

Bexarotene Displays Weak Binding Propensity to $\text{A}\beta_{1-42}$ Monomer. Because intrinsically disordered $\text{A}\beta_{1-42}$ peptide has no structure available in PDB, we have adopted the ensemble-based approach to compute ΔG_{bind} . Namely, instead of a single target, we used nine representative structures generated in MD simulations²⁶ as putative targets (Figure S11). First, we have docked bexarotene to these structures, and the best docking conformations (Figure S11) were used as starting configurations for the MD simulations.

As follows from the time dependence of RMSD (Figure S12), the complexes reached equilibrium at different times ranging from about 50 to 240 ns. Snapshots obtained at equilibrium (i.e., after the arrow in Figure S12) were used to estimate the binding free energy. As in the case of $5\text{A}\beta_{17-42}$ protofibril, for all studied models the vdW interaction dominates over the electrostatic interaction as $|\Delta E_{\text{vdw}}| > |\Delta E_{\text{ele}}|$ (Table S5). Contrary to the polar contribution (ΔG_{PB}), the nonpolar (ΔG_{sur}) and entropy ($T\Delta S$) terms are not sensitive to starting conformations. Overall, bexarotene is weakly bound to $\text{A}\beta_{1-42}$ monomer with mean $\Delta G_{\text{bind}} \approx -1.8$ kcal/mol (Table 1) implying that the prolongation of the nucleation step is not caused by binding of single bexarotene to monomer.

Residues Glu11, Lys16, Glu23, Lys28, and Gly29 give a significant contribution to the electric interaction between bexarotene and monomer (Figure S13). Except Gly29 the other residues are charged. Negatively charged residue Asp7 experiences a repulsive force from bexarotene. We highlight the role of Glu23 and Lys28 that form the salt bridge which plays a key role in fibril formation.²⁷ Residues Lys16, Phe19, Phe20, Ile31, Ile32, Leu34 Val36, Val39, Val40, and Ile41 are dominating in the vdW interaction (Figure S13). Combining the electrostatic and vdW interactions one can see that residues

Table 2. Secondary Structures (%) of $\text{A}\beta_{1-42}$ and $\text{A}\beta_{1-42} + 10$ Bexarotenes^a

systems	β -content	helix	turn	coil
$\text{A}\beta_{1-42}$	10.8 ± 2.6	3.5 ± 0.9	17.4 ± 6.8	68.3 ± 9.7
$\text{A}\beta_{1-42} + 10$ bexarotenes	4.7 ± 2.3	0.6 ± 2.2	16.3 ± 6.1	78.4 ± 6.5

^aResults were obtained by REMD method.

Lys16, Phe19, Phe20, Ile31, Ile32, Leu34, Val39, Val40, and Ile41 govern the binding of bexarotene.

Using the docking method, Mirza et al.²⁸ have shown that residues His13 and Lys 16 are crucial for the interaction with bexarotene. This result is partially consistent with our finding on the important role of residue Lys16. Contrary to our in silico and in vitro results, Mirza et al.²⁸ reported that bexarotene strongly binds to $\text{A}\beta_{42}$ monomer. This difference is presumably due to different methods that we have used the all-atom MD simulation while the structural bioinformatics method was employed by those authors.

Low Binding Affinity of Bexarotene to Dimer. Molecular structures of $\text{A}\beta$ oligomers of different sizes were obtained by MD simulations, but only dimers have been studied thoroughly.²⁹ To compute the binding free energy, we have employed the MD structure of $\text{A}\beta_{1-42}$ dimer obtained by Zhang et al.³⁰ because in contrast to other models, the reliability of this structure was confirmed by pulling experiment.

Four independent MD runs have been carried out. Trajectories 1–3 were started from structures obtained in three binding modes with the lowest energies (Figure S14), whereas trajectory 4 has the same initial structure as trajectory 1 but with a different seed number. The equilibration times, marked by arrows in Figure S15, vary between about 40 ns (trajectory 3) and 160 ns (trajectory 1). The binding free energies computed in equilibrium for 4 trajectories are listed in Table S6. As in the protofibril and monomer cases the electrostatic interaction is less important than the vdW interaction and the polar term strongly depends on starting configurations. With the mean $\Delta G_{\text{bind}} \approx 0.6$ kcal/mol, bexarotene does not prefer to bind to dimers suggesting that, consistent with the data in Figure 3, bexarotene delays the fibril growth not through binding to oligomers at low bexarotene concentrations (in the dimer case the bexarotene: $\text{A}\beta$ ratio is 1:2).

Prolongation of the Lag Phase through Reduction of the β -Content of Monomer at High Bexarotene Concentrations. In the in vitro experiment, the impact of bexarotene on the lag phase is clearly seen at high enough bexarotene concentrations (Figure 4), and thus, we have considered the case with bexarotene: $\text{A}\beta$ ratio 10:1. The 200 ns REMD simulations with 64 replicas (see details in SI) were carried out starting from the configuration where 10 bexarotenes were positioned around $\text{A}\beta_{1-42}$ monomer (Figure 1C). The data analysis was made at $T = 300.43$ K. Clearly, both systems reached equilibrium at ≈ 80 ns (Figure S16). The secondary structures obtained at equilibrium are shown in Table 2.

Using filtration through 10 000 molecular weight cutoff, circular dichroism (CD) of all low molecular weight $\text{A}\beta_{42}$ aggregates gives 11% of β -strand, 3% of α -helix, and 86% of coil +turn at 295 K, pH 7.5.³¹ This result is in excellent agreement with our data (Table 2). Our 11% of β -strand is not far from 15% obtained by the MD simulation of Head-Gordon et al.³² but lower than 21% reported by Viet et al.³³ using the OPLS-AA force field and the TIP3P water model. Using the

AMBER99sb-ILDN force field and TIP4P-Ew water model, Rosenman et al. obtained $\beta \approx 23\%$.³⁴

In the presence of 10 bexarotenes, the β -content is reduced from 11% to 5%. This effect is also evident from the representative structures obtained for two systems (Figure S17) using the clustering method.³⁵ Based on RMSD, all snapshots were grouped into 20 clusters, and the 3 most populated clusters were picked up. In $\text{A}\beta_{42}$, they have populations of 23.9, 17.9, and 15%. The corresponding structures possess 14.3, 9.5, and 9.5% of β -strand which are higher than 4.8% of the representative structures of $\text{A}\beta_{42} + 10$ bexarotenes. The helix is only populated in structure 2 of $\text{A}\beta_{42}$ (Figure S17). Note that for each individual system the representative structures have nearly the same β -content but being mainly different in turn and coil (Figure S17).

In the presence of bexarotene, the substantial decrease in β -strand occurs at residues 11, 12, 31, and 32, while it levels up at residues 17 and 41 (Figure 6). The helix is poorly populated in

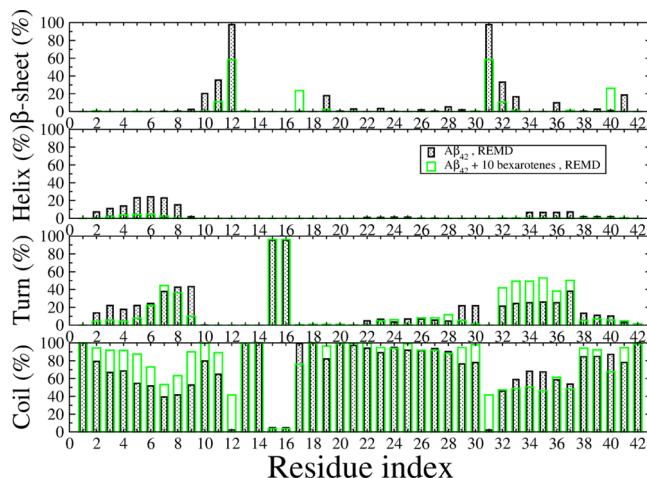


Figure 6. Per-residue distributions of secondary structures of $\text{A}\beta_{1-42}$ monomer without and with 10 bexarotenes. Results were obtained by the all-atom REMD simulation.

$\text{A}\beta_{42}$ (3.5%) as well as in $\text{A}\beta_{42} + 10$ bexarotenes (0.6%) (Table 2 and Figure 6). Upon bexarotene binding, the coil increases by about 10% mainly at the N-terminus (Figure 6) with the turn remaining almost unchanged.

Because the monomer can serve as a template for nucleation in formation of fibrils with cross- β structures, the propensity to self-assembly is controlled by the population of the fibril-prone state of monomer³⁶ or by the β -content of $\text{A}\beta$ peptides. Thus, the β -content reduction by bexarotene (Table 2) implies that at high enough concentrations this ligand delays the fibril growth, consistent with ours (Figure 4) and Habchi et al. experiments.²¹ The increase in coil at the N-terminal also provides an additional evidence for the slower aggregation. Thus, our REMD simulations revealed the molecular mechanism for prolongation of the lag phase by bexarotene.

Why One Needs High Concentrations To Clearly Observe the Delay Effect? In order to answer this question, we show a movie obtained by the REMD simulation at 300 K for $\text{A}\beta_{1-42}$ in complex with 10 bexarotenes (Movie 1 in SI). Clearly, bexarotene has very high propensity to self-assembly leading to weak impact on $\text{A}\beta$ structures if its concentration is not high enough. This phenomenon is even more evident from conventional 1000 ns MD runs (not REMD) as demonstrated in Movie 2 in SI.

MATERIAL AND METHODS

Chemicals. Synthetic human amyloid- β_{1-42} (lot no. 08161342 T) was purchased from rPeptide (U.S.A.). The peptide concentration was determined spectrophotometrically (Jasco V-630 Spectrophotometer) using an extinction coefficient of 38 940 M⁻¹ cm⁻¹ at $\lambda = 276$ nm. Bexarotene was obtained from Sigma-Aldrich (St. Louis, MO, U.S.A.), and stock solution was prepared by dissolving of the compound in 100% dimethyl sulfoxide (DMSO) to a concentration of 50 mM. Thioflavin T (ThT), 1,1,1,3,3,3-Hexafluoroisopropanol (HFIP), hydrochloric acid (HCl, 36%), dimethyl sulfoxide (DMSO), and sodium azide (NaN₃) were obtained from Sigma-Aldrich and were of analytical reagent grade.

$\text{A}\beta_{1-42}$ Peptide Amyloid Fibrilization. $\text{A}\beta_{1-42}$ amyloid fibrils were prepared as described by Stine et al.³⁷ Briefly, $\text{A}\beta_{1-42}$ was dissolved in HFIP to 1 mM concentration, and subsequently, the HFIP was evaporated. The thin film of $\text{A}\beta_{1-42}$ peptide was dissolved in 20 μL of DMSO to obtain a 5 mM stock solution of $\text{A}\beta_{1-42}$. Solution was centrifuged (14 000 rpm, 30 s) and sonicated for 10 min in a bath sonicator.

Formation of amyloid fibrils was achieved by 8 days incubation of 10 μM $\text{A}\beta_{1-42}$ in 10 mM HCl solution at 37 °C. The extent of $\text{A}\beta_{1-42}$ amyloid fibrilization and presence of amyloid fibrils were monitored by characteristic changes in Thioflavin T fluorescence intensity using ThT assay. Morphology and characteristics of fibrils were evaluated using atomic force microscopy (AFM).

Thioflavin T (ThT) Fluorescence Assay. The presence of amyloid fibrils is detected as a significant enhancement of ThT fluorescence. Thioflavin T was added to $\text{A}\beta_{1-42}$ samples (10 μM) to a final concentration of 20 μM , and the samples were incubated at 37 °C for 1 h. Fluorescence intensity was measured in a black, low-binding nontransparent polyethylene glycol coating 96-well plate using a Synergy MX (BioTek Company, U.S.A.) spectrofluorimeter. The excitation wavelength was set at 440 nm, and the emission was recorded at 485 nm. The emission slits were adjusted to 9.0/9.0 nm, and the top probe vertical offset was 6 mm. All ThT fluorescence experiments were performed in triplicate, and the final value is the average of measured values.

Interference of the Bexarotene with $\text{A}\beta_{1-42}$ Amyloid Fibrilization and Amyloid Fibrils. The ability of bexarotene to interfere with amyloid aggregation was studied using ThT assay. The inhibitory effect of bexarotene on amyloid fibrilization of the $\text{A}\beta_{1-42}$ was studied at different concentrations of bexarotene (from 100 pM to 1M) and 10 μM of $\text{A}\beta_{1-42}$ solution. Effect of bexarotene on $\text{A}\beta_{1-42}$ fibrils (10 μM) was examined after their 24 h incubation at 37 °C for concentration range from 100 pM to 1 mM. As a control, the protein was replaced with buffer to measure the fluorescence of bexarotene. All data were normalized to ThT fluorescence determined for $\text{A}\beta_{1-42}$ aggregates alone (100%). Each experiment was performed in triplicate, and the final value is the average of the measured values.

Atomic Force Microscopy (AFM). $\text{A}\beta_{1-42}$ samples containing 10 mM HCl solution and bexarotene were directly deposited onto freshly cleaved mica and left to absorb on the surface. Then the substrate was rinsed with ultrapure water (Purelab Flex, Veolia Water) and air-dried prior to scan. AFM images were acquired using a Scanning Probe Microscope (Veeco di Innova). The instrument was operated in tapping mode under ambient conditions using rectangular uncoated silicon cantilever NCHV (Bruker AFM Probes with a specific resistance of 0.01–0.025 Ω cm, antimony (n)-doped Si), with a typical

resonance frequency 320 kHz and a force constant 42 N/m. No smoothing or noise reduction was applied.

Kinetic Measurement of the Bexarotene Ability To Affect $\text{A}\beta_{1-42}$ Fibrillization. For kinetic measurements, different concentrations of bexarotene (10, 50, and 100 μM) were added to 10 μM $\text{A}\beta_{1-42}$ native peptide, and the mixture was incubated at 37 °C for 8 days. To evaluate the effect of bexarotene on the process of $\text{A}\beta_{1-42}$ fibril formation, Thioflavin T was added to aliquots that were withdrawn at varying times. Every experiment was performed in triplicate, and the reported values are the averages of measured data, with the error bars representing the average deviation. The growth curves were obtained by fitting the average values by nonlinear least-squares method.

Structure of Bexarotene. The recent data about Bexarotene obtained from Open Chemistry Database (<https://pubchem.ncbi.nlm.nih.gov/compound/Bexarotene#section=Top>) point out that this compound is only found in individuals that have used or taken this drug for treatment. It is an antineoplastic agent indicated by the FDA for Cutaneous T cell lymphoma (CTCL).³⁸ The exact mechanism of action of bexarotene in the treatment of CTCL is unknown, but the drug has activity in all clinical stages of CTCL (<http://www.hmdb.ca/metabolites/HMDB14452>).

Four bexarotene metabolites have been identified in plasma: 6- and 7-hydroxy-bexarotene and 6- and 7-oxo-bexarotene. In vitro studies suggest that after oxidation, metabolites may be glucuronidated. The oxidative metabolites are active in the in vitro assays of retinoid receptor activation, but the relative contribution of the parent and any metabolites to the efficacy and safety of bexarotene is unknown (<http://toxnet.nlm.nih.gov/cgi-bin/sis/search/r?dbs+hsdb:@term+@rn+@rel+153559-49-0>). Moreover, the uptake of bexarotene by organs (brain) or tissues has not been evaluated. We assume that bexarotene can be metabolized in brain, but as Howel et al. have shown, the abundance of the 6-hydroxy-bexarotene metabolite was greater than that of the parent in plasma of patients with advanced cancer. The abundance of 6-/7-oxo metabolite was lower than that or equivalent to that of the parent.³⁹

The pK_a constant for bexarotene is equal to 4.2 (carboxylic acid) (obtained from Open Chemistry Database, <http://toxnet.nlm.nih.gov/cgi-bin/sis/search/r?dbs+hsdb:@term+@rn+@rel+153559-49-0>) suggesting that bexarotene is most likely presented in the deprotonated form in CSF as pH of CSF is about 7.3.

Therefore, for simulation, we considered bexarotene in the neutral form. Then the chemical formula of bexarotene is $\text{C}_{24}\text{H}_{28}\text{O}_2$, and its 2D structure is shown in Figure 1a. For molecular simulation, the 3D structure was first built by GaussView5 and then optimized using GAUSSIAN09 package.⁴⁰

Structures of Targets. The question about polymorphic fibril structures of $\text{A}\beta$ peptides is still under hot debate. However, 16 residues of $\text{A}\beta_{1-42}$ at N-terminal, which are believed to be disordered in the fibrillar state, are neglected in the construction of fibril structure. For simulations the fibril model for truncated peptides $\text{A}\beta_{17-42}$, resolved by the solid-state NMR technique $\text{A}\beta_{17-42}$ fibril⁵ (PDB ID: 2BEG, Figure 1b) is widely used (see, for instance⁴¹ and references therein). Here we have also performed molecular simulations using this structure. The binding site of $5\text{A}\beta_{17-42}$ fibril has not been experimentally determined yet,⁴¹ and it is determined from docking simulation. For REMD simulation, the $\text{A}\beta_{1-42}$ monomer structure was taken from previous simulations, and 10 bexarotenes were randomly positioned around it (Figure 1c).

Docking Method. To dock bexarotene to the $5\text{A}\beta_{17-42}$ fibril the PDBQT files for receptor and ligand were prepared using AutodockTools 1.5.4.⁴² Autodock4 force fields and Gasteiger charges were used for both ligand and receptor. Autodock Vina⁴³ has been employed for estimation of binding energy. For global search, the exhaustiveness was set to equal 400, and the maximum difference between energies of the best and worse binding modes was chosen as large as 7 kcal/mol. Twenty binding modes were generated starting from random configurations of ligand. The receptor was kept fixed, while the dynamics of ligand was fully allowed. In the $5\text{A}\beta_{17-42}$ case,

we placed the grid's center at the protofibril center with the grid dimensions of $36 \times 35 \times 55 \text{ \AA}^3$ covering the whole target.

Molecular Dynamic (MD) Simulation. A semiempirical quantum chemistry program (SQM) was used to optimize bexarotene structure and calculate AM1-bcc charge. Parmchk was used to read in gaff force field files from which the parameters are taken to describe bond, angle, dihedral, improper, and nonbonded interactions for bexarotene. Atom types and charges are provided in the file *Bexa_atomtype_charge.docx* and the force field parameters in *BEX.docx* in Supporting Information (SI).

For protein, the AMBER force field 99SB⁴⁴ implemented in Amber14 package^{45,46} was employed together with water model TIP3P⁴⁷ for all-atom MD simulation. One can show that TIP3 model is the most suitable for the AMBER force field.^{48,49} The structures, shown in Figure 1, S4, S6, S8, S11, and S14 were utilized as initial structures for MD runs. The leapfrog algorithm⁵⁰ was used to solve Langevin equations of motion with a time step $\Delta t = 2 \text{ fs}$. By the SHAKE algorithm,⁵¹ the length constraint on bonds associated with hydrogen atom was imposed. Temperature was maintained by the Langevin thermostat⁵² having a frequency of collision equal to 2 ps^{-1} . A cutoff of 1.4 nm was used to estimate vdW forces, while long-range electrostatic interactions were computed by the PME (particle mesh Ewald) method.⁵³ The production runs were performed in the NPT mode.

MM-PBSA Method. Neglecting receptor dynamics and restricting to a limited number of trial positions for ligand the predictive power of the docking method rather weak. Therefore, a more accurate MM-PBSA method was applied to refine binding affinity obtained by the docking simulation for bexarotene. The details of this method are available in our previous works.^{54–56} In the MM-PBSA method one can estimate the binding free energy ΔG_{bind} of a small molecule to target by the following equation:

$$\Delta G_{\text{bind}} = \Delta E_{\text{elec}} + \Delta E_{\text{vdW}} + \Delta G_{\text{sur}} + \Delta G_{\text{PB}} - T\Delta S \quad (1)$$

Here ΔE_{vdW} and ΔE_{elec} refer to vdW and electrostatic interactions. ΔG_{sur} is nonpolar, while ΔG_{PB} is polar energy of solvation. The entropic term $T\Delta S$ was computed in the so-called normal mode approximation.⁵⁷ Equilibrium phase snapshots and eq 1 were used to compute ΔG_{bind} .

In more detail, we used MMPBSA.py⁵⁸ tools in the AMBER package to calculate the binding free energy, mmpbsa_py_nabnmode was used to calculate entropic contribution, while mmpbsa_py_energy was employed to compute the remaining terms with the force field used in the simulation. In the normal mode approximation calculation, the HCT Generalized Born solvation model^{59,60} was used (nmode_igb = 1) with ionic strength nmod_istrng = 0.1, the convergence criterion for the energy minimization (drms) is set to 0.0001 and the maximal minimization step (maxcyc) is set to 50 000.

In the solvation free energy (PB) calculation, PBSA solver was used instead of APBS to solve the Poisson–Boltzmann equation for the electrostatic term (GPB), and the hydrophobic term is defined as

$$G_{\text{sur}} = \alpha * \text{SASA} + \beta \quad (2)$$

where cavity surface tension α is 0.005, the cavity offset β is 0.000, and the solvent accessible surface area (SASA) is approximated by LCPO method.⁶¹

Tools and Measures Used for Data Analysis. A hydrogen bond (HB) was formed provided the distance between donor D and acceptor A is $<3.5 \text{ \AA}$, the H–A distance is $<2.7 \text{ \AA}$ and the D–H–A angle is >135 degrees. A nonbonded contact (NBC) is a noncovalent bonded contact except HB. It is defined as contact between atom C or S of ligand and any atom of either protein or water molecule when they are far away by distances 2.9–3.9 \AA . The HBs and NBCs were analyzed using LigPlot++ version 1.44.⁶²

CONCLUSION

Because of a possible important role of bexarotene in treatment of AD we have carefully studied its impact on $A\beta_{1-42}$ self-assembly. Our in vitro experiments disclosed that bexarotene

does not reverse the fibrillation but it can delay the self-assembly process. By all-atom MD simulations in explicit water for the first time we have disclosed the molecular mechanisms underlying these phenomena. Namely, bexarotene is not capable to clear fibrils due to its low binding affinity, while the prolongation of the lag phase is associated with the reduction of β -sheet content in monomer state. In addition, the delay in fibril growth, observed only at high bexarotene concentrations, is due to high propensity of bexarotene to self-assembly. Overall, our findings are in agreement with some in vivo experiments showing that bexarotene does not clear $A\beta$ fibrils.^{14–16,18,19} From this prospect, the clearance is presumably due to the bexarotene-induced enhancement of ApoE association with lipoproteins in mouse models or by other unknown mechanisms.

Recently the impact of bexarotene derivatives on the behavior of retinoid X-receptor has been investigated by MD and molecular flooding simulations.⁶³ It would be interesting to carry out a similar study for $A\beta$ aggregation to screen out potent drug candidates for AD.

ASSOCIATED CONTENT

Supporting Information

The Supporting Information is available free of charge on the ACS Publications website at DOI: 10.1021/acscchemneuro.7b00107.

Binding free energy of bexarotene to monomer, dimer, and protofibril; HB and nonbonded contact network of $5A\beta_{17-42}$ and bexarotene in the best docking mode; the time dependence of RMSD for $A\beta_{1-42}$ +bexarotene, $2A\beta_{1-42}$ +bexarotene, $5A\beta_{17-42}$, and $5A\beta_{17-42}+6$ bexarotenes; details of MM-PBSA simulation of binding affinity of bexarotene to 2MXU, SKK3, and 2NAO fibrils; details of REMD simulations for $A\beta_{1-42}+10$ bexarotenes and bexarotene bound to dimer (PDF)

Atom types and charges (PDF)

Force field parameters (PDF)

REMD simulation at 300 K (AVI)

1000 ns MD runs (AVI)

AUTHOR INFORMATION

Corresponding Authors

*E-mail: masli@ifpan.edu.pl. Phone: +48 22 843 66 01.

*E-mail: gazova@saske.sk. Phone: +421 55 7204 131.

ORCID

Mai Suan Li: 0000-0001-7021-7916

Author Contributions

¶P.D.Q.H., N.Q.T., and L.H.P. contributed equally. M.S.L., N.Q.T., and Z.G. conceived the experiments. P.D.Q.H., N.Q.T., Z.B., and L.H.P. conducted the experiment. P.D.Q.H., N.Q.T., Z.B., L.H.P., Z.G., and M.S.L. analyzed the results. M.S.L., Z.G., Z.B., P.D.Q.H., and N.Q.T. wrote the paper. All authors reviewed the manuscript.

Funding

This work was supported by Narodowe Centrum Nauki in Poland (grant no. 2015/19/B/ST4/02721), and Department of Science and Technology at Ho Chi Minh City, Vietnam. Allocation of CPU time at the supercomputer center TASK in Gdansk (Poland) is highly appreciated. In Slovakia the work was supported by research grants SAS-MOST JRP2015/S,

VEGA 2/0145/17, 2/0175/14 and MVTS NGP-NET-BM140S.

Notes

The authors declare no competing financial interest.

ACKNOWLEDGMENTS

Department of Science and Technology at Ho Chi Minh city, Vietnam, Narodowe Centrum Nauki (NCN) in Poland, and the supercomputer center TASK in Gdansk, Poland.

REFERENCES

- (1) Henderson, A. S., and Jorm, A. F. Definition and Epidemiology of Dementia: A Review. In *Dementia*; Maj, M., and Sartorius, N., Eds.; John Wiley & Sons, Ltd: Chichester, U.K., 2002; pp 1–68.
- (2) Hardy, J., and Selkoe, D. J. (2002) The amyloid hypothesis of Alzheimer's disease: progress and problems on the road to therapeutics. *Science* **297**, 353–356.
- (3) Nasica-Labouze, J., Nguyen, P. H., Sterpone, F., Berthoumieu, O., Buchete, N.-V., Coté, S. b., De Simone, A., Doig, A. J., Faller, P., Garcia, A., et al. (2015) Amyloid β protein and Alzheimer's disease: When computer simulations complement experimental studies. *Chem. Rev.* **115**, 3518–3563.
- (4) Petkova, A. T., Ishii, Y., Balbach, J. J., Antzutkin, O. N., Leapman, R. D., Delaglio, F., and Tycko, R. (2002) A structural model for Alzheimer's β -amyloid fibrils based on experimental constraints from solid state NMR. *Proc. Natl. Acad. Sci. U. S. A.* **99**, 16742–16747.
- (5) Lührs, T., Ritter, C., Adrian, M., Riek-Loher, D., Bohrmann, B., Döbeli, H., Schubert, D., and Riek, R. (2005) 3D structure of Alzheimer's amyloid- β (1–42) fibrils. *Proc. Natl. Acad. Sci. U. S. A.* **102**, 17342–17347.
- (6) Kayed, R., Head, E., Thompson, J. L., McIntire, T. M., Milton, S. C., Cotman, C. W., and Glabe, C. G. (2003) Common structure of soluble amyloid oligomers implies common mechanism of pathogenesis. *Science* **300**, 486–489.
- (7) Citron, M. (2004) Strategies for disease modification in Alzheimer's disease. *Nat. Rev. Neurosci.* **5**, 677–685.
- (8) Wood, A. J. J., and Cummings, J. L. (2004) Alzheimer's Disease. *N. Engl. J. Med.* **351**, 56–67.
- (9) Gniadecki, R., Assaf, C., Bagot, M., Dummer, R., Duvic, M., Knobler, R., Ranki, A., Schwandt, P., and Whittaker, S. (2007) The optimal use of bexarotene in cutaneous T-cell lymphoma. *Br. J. Dermatol.* **157**, 433–440.
- (10) Cramer, P. E., Cirrito, J. R., Wesson, D. W., Lee, C. D., Karlo, J. C., Zinn, A. E., Casali, B. T., Restivo, J. L., Goebel, W. D., James, M. J., et al. (2012) ApoE-directed therapeutics rapidly clear β -amyloid and reverse deficits in AD mouse models. *Science* **335**, 1503–1506.
- (11) Cramer, P. E., Cirrito, J. R., Wesson, D. W., Lee, C. D., Karlo, J. C., Zinn, A. E., Casali, B. T., Restivo, J. L., Goebel, W. D., James, M. J., et al. (2012) ApoE-directed therapeutics rapidly clear β -amyloid and reverse deficits in AD mouse models. *Science* **335**, 1503–1506.
- (12) Savage, J. C., Jay, T., Goduni, E., Quigley, C., Mariani, M. M., Malm, T., Ransohoff, R. M., Lamb, B. T., and Landreth, G. E. (2015) Nuclear Receptors License Phagocytosis by Trem2(+) Myeloid Cells in Mouse Models of Alzheimer's Disease. *J. Neurosci.* **35**, 6532–6543.
- (13) Mariani, M. M., Malm, T., Lamb, R., Jay, T. R., Neilson, L., Casali, B., Medarametla, L., and Landreth, G. E. (2017) Neuronally-directed effects of RXR activation in a mouse model of Alzheimer's disease. *Sci. Rep.* **7**, 42270.
- (14) Fitz, N. F., Cronican, A. A., Lefterov, I., and Koldamova, R. (2013) Comment on "ApoE-Directed Therapeutics Rapidly Clear β -Amyloid and Reverse Deficits in AD Mouse Models". *Science* **340**, 924–924.
- (15) Price, A. R., Xu, G., Sieminski, Z. B., Smithson, L. A., Borchelt, D. R., Golde, T. E., and Felsenstein, K. M. (2013) Comment on "ApoE-Directed Therapeutics Rapidly Clear β -Amyloid and Reverse Deficits in AD Mouse Models". *Science* **340**, 924–924.
- (16) Tesseur, I., Lo, A. C., Roberfroid, A., Dietvorst, S., Van Broeck, B., Borgers, M., Gijsen, H., Moechars, D., Mercken, M., Kemp, J., D'Hooge, R., and De Strooper, B. (2013) Comment on "ApoE-Directed Therapeutics Rapidly Clear β -Amyloid and Reverse Deficits in AD Mouse Models". *Science* **340**, 924–924.
- (17) Veeraraghavalu, K., Zhang, C., Miller, S., Hefendehl, J. K., Rajapaksha, T. W., Ulrich, J., Jucker, M., Holtzman, D. M., Tanzi, R. E., Vassar, R., and Sisodia, S. S. (2013) Comment on "ApoE-Directed Therapeutics Rapidly Clear β -Amyloid and Reverse Deficits in AD Mouse Models". *Science* **340**, 924–924.
- (18) Ghosal, K., Haag, M., Verghese, P. B., West, T., Veenstra, T., Braunstein, J. B., Bateman, R. J., Holtzman, D. M., and Landreth, G. E. (2016) A randomized controlled study to evaluate the effect of bexarotene on amyloid- β and apolipoprotein E metabolism in healthy subjects. *Alzheimer's Dementia: Translational Research & Clinical Interventions* **2**, 110–120.
- (19) O'Hare, E., Jeggo, R., Kim, E. M., Barbour, B., Walczak, J. S., Palmer, P., Lyons, T., Page, D., Hanna, D., Meara, J. R., Spanswick, D., Guo, J. P., McGeer, E. G., McGeer, P. L., and Hobson, P. (2016) Lack of support for bexarotene as a treatment for Alzheimer's disease. *Neuropharmacology* **100**, 124–130.
- (20) Kollman, P. A., Massova, I., Reyes, C., Kuhn, B., Huo, S., Chong, L., Lee, M., Lee, T., Duan, Y., Wang, W., et al. (2000) Calculating structures and free energies of complex molecules: combining molecular mechanics and continuum models. *Acc. Chem. Res.* **33**, 889–897.
- (21) Habchi, J., Arosio, P., Perni, M., Costa, A. R., Yagi-Utsumi, M., Joshi, P., Chia, S., Cohen, S. I. A., Muller, M. B. D., Linse, S., Nollen, E. A. A., Dobson, C. M., Knowles, T. P. J., and Vendruscolo, M. (2016) An anticancer drug suppresses the primary nucleation reaction that initiates the production of the toxic A beta 42 aggregates linked with Alzheimer's disease. *Science Advances* **2**, e1501244.
- (22) Xiao, Y. L., Ma, B. Y., McElheny, D., Parthasarathy, S., Long, F., Hoshi, M., Nussinov, R., and Ishii, Y. (2015) A beta(1–42) fibril structure illuminates self-recognition and replication of amyloid in Alzheimer's disease. *Nat. Struct. Mol. Biol.* **22**, 499–U497.
- (23) Colvin, M. T., Silvers, R., Ni, Q. Z., Can, T. V., Sergeyev, I., Rosay, M., Donovan, K. J., Michael, B., Wall, J., Linse, S., and Griffin, R. G. (2016) Atomic Resolution Structure of Monomorphic A beta(42) Amyloid Fibrils. *J. Am. Chem. Soc.* **138**, 9663–9674.
- (24) Walti, M. A., Ravotti, F., Arai, H., Glabe, C. G., Wall, J. S., Bockmann, A., Guntert, P., Meier, B. H., and Riek, R. (2016) Atomic-resolution structure of a disease-relevant A beta(1–42) amyloid fibril. *Proc. Natl. Acad. Sci. U. S. A.* **113**, E4976–E4984.
- (25) Tycko, R. (2016) Alzheimer's disease: Structure of aggregates revealed. *Nature* **537**, 492.
- (26) Yang, M. F., and Teplow, D. B. (2008) Amyloid beta-Protein Monomer Folding: Free-Energy Surfaces Reveal Alloform-Specific Differences. *J. Mol. Biol.* **384**, 450–464.
- (27) Nasica-Labouze, J., Nguyen, P. H., Sterpone, F., Berthoumieu, O., Buchete, N.-V., Coté, S. b., De Simone, A., Doig, A. J., Faller, P., Garcia, A., et al. (2015) Amyloid β protein and Alzheimer's disease: When computer simulations complement experimental studies. *Chem. Rev.* **115**, 3518–3563.
- (28) Mirza, Z., and Amin Beg, M. (2017) Possible Molecular Interactions of Bexarotene - A Retinoid Drug and Alzheimer's Peptide: A Docking Study. *Current Alzheimer Research* **14**, 327–334.
- (29) Nagel-Steger, L., Owen, M. C., and Strodel, B. (2016) An Account of Amyloid Oligomers: Facts and Figures Obtained from Experiments and Simulations. *ChemBioChem* **17**, 657–676.
- (30) Zhang, Y. L., Hashemi, M., Lv, Z. J., and Lyubchenko, Y. L. (2016) Self-assembly of the full-length amyloid A beta 42 protein in dimers. *Nanoscale* **8**, 18928–18937.
- (31) Kirkitadze, M. D., Condron, M. M., and Teplow, D. B. (2001) Identification and characterization of key kinetic intermediates in amyloid beta-protein fibrillogenesis. *J. Mol. Biol.* **312**, 1103–1119.

- (32) Ball, K. A., Phillips, A. H., Wemmer, D. E., and Head-Gordon, T. (2013) Differences in beta-strand Populations of Monomeric A beta 40 and A beta 42. *Biophys. J.* 104, 2714–2724.
- (33) Viet, M. H., Nguyen, P. H., Ngo, S. T., Li, M. S., and Derreumaux, P. (2013) Effect of the Tottori Familial Disease Mutation (D7N) on the Monomers and Dimers of A beta(40) and A beta(42). *ACS Chem. Neurosci.* 4, 1446–1457.
- (34) Rosenman, D. J., Wang, C. Y., and Garcia, A. E. (2016) Characterization of A beta Monomers through the Convergence of Ensemble Properties among Simulations with Multiple Force Fields. *J. Phys. Chem. B* 120, 259–277.
- (35) Roe, D. R., and Cheatham, T. E. (2013) PTraj and CPPTRAJ: Software for Processing and Analysis of Molecular Dynamics Trajectory Data. *J. Chem. Theory Comput.* 9, 3084–3095.
- (36) Li, M. S., Co, N. T., Reddy, G., Hu, C. K., Straub, J. E., and Thirumalai, D. (2010) Factors Governing Fibrillogenesis of Polypeptide Chains Revealed by Lattice Models. *Phys. Rev. Lett.* 105, 218101.
- (37) Stine, W. B., Jungbauer, L., Yu, C., and LaDu, M. J. (2010) *Methods Mol. Biol.* 670, 13–32.
- (38) Scarisbrick, J. J., Morris, S., Azurdia, R., Illidge, T., Parry, E., Graham-Brown, R., Cowan, R., Gallop-Evans, E., Wachsmuth, R., Eagle, M., Wierzbicki, A. S., Soran, H., Whittaker, S., and Wain, E. M. (2013) UK consensus statement on safe clinical prescribing of bexarotene for patients with cutaneous T-cell lymphoma. *Br. J. Dermatol.* 168, 192–200.
- (39) Howell, S. R., Shirley, M. A., Grese, T. A., Neel, D. A., Wells, K. E., and Ulm, E. H. (2001) Bexarotene metabolism in rat, dog, and human, synthesis of oxidative metabolites, and in vitro activity at retinoid receptors. *Drug Metab. Dispos.* 29, 990–998.
- (40) Frisch, M., Trucks, G., Schlegel, H., Scuseria, G., Robb, M., Cheeseman, J., Scalmani, G., Barone, V., Mennucci, B., and Petersson, G. et al. Gaussian 09, revision D.01. Gaussian, Inc.: Wallingford CT, 2009.
- (41) Huy, P. D. Q., and Li, M. S. (2014) Binding of fullerenes to amyloid beta fibrils: size matters. *Phys. Chem. Chem. Phys.* 16, 20030–20040.
- (42) Sanner, M. F. (1999) Python: a programming language for software integration and development. *J. Mol. Graph Model* 17, 57–61.
- (43) Trott, O., and Olson, A. J. (2010) AutoDock Vina: improving the speed and accuracy of docking with a new scoring function, efficient optimization, and multithreading. *Journal of computational chemistry* 31, 455–461.
- (44) Hornak, V., Abel, R., Okur, A., Strockbine, B., Roitberg, A., and Simmerling, C. (2006) Comparison of multiple Amber force fields and development of improved protein backbone parameters. *Proteins: Struct., Funct., Genet.* 65, 712–725.
- (45) Pearlman, D. A., Case, D. A., Caldwell, J. W., Ross, W. S., Cheatham, T. E., DeBolt, S., Ferguson, D., Seibel, G., and Kollman, P. (1995) AMBER, a package of computer programs for applying molecular mechanics, normal mode analysis, molecular dynamics and free energy calculations to simulate the structural and energetic properties of molecules. *Comput. Phys. Commun.* 91, 1–41.
- (46) Case, D. A., Cheatham, T. E., Darden, T., Gohlke, H., Luo, R., Merz, K. M., Onufriev, A., Simmerling, C., Wang, B., and Woods, R. J. (2005) The Amber biomolecular simulation programs. *J. Comput. Chem.* 26, 1668–1688.
- (47) Jorgensen, W. L., Chandrasekhar, J., Madura, J. D., Impey, R. W., and Klein, M. L. (1983) Comparison of simple potential functions for simulating liquid water. *J. Chem. Phys.* 79, 926–935.
- (48) van Gunsteren, W. F., Billeter, S. R., Eising, A. A., Hünenberger, P. H., Krüger, P., Mark, A. E., Scott, W. R., and Tironi, I. G. *Biomolecular Simulation: The {GROMOS96} Manual and User Guide*; Vdf Hochschulverlag AG an der ETH Zürich: Zürich, Switzerland, 1996.
- (49) Nguyen, T. T., Viet, M. H., and Li, M. S. (2014) Effects of water models on binding affinity: evidence from all-atom simulation of binding of tamiflu to A/H5N1 neuraminidase. *Sci. World J.* 2014, 1.
- (50) Hockney, R., Goel, S., and Eastwood, J. (1974) Quiet high-resolution computer models of a plasma. *J. Comput. Phys.* 14, 148–158.
- (51) Ryckaert, J.-P., Ciccotti, G., and Berendsen, H. J. (1977) Numerical integration of the cartesian equations of motion of a system with constraints: molecular dynamics of n-alkanes. *J. Comput. Phys.* 23, 327–341.
- (52) Wu, X., and Brooks, B. R. (2003) Self-guided Langevin dynamics simulation method. *Chem. Phys. Lett.* 381, 512–518.
- (53) Darden, T., York, D., and Pedersen, L. (1993) Particle mesh Ewald: An N· log (N) method for Ewald sums in large systems. *J. Chem. Phys.* 98, 10089–10092.
- (54) Ngo, S. T., and Li, M. S. (2012) Curcumin binds to A β 1–40 peptides and fibrils stronger than ibuprofen and naproxen. *J. Phys. Chem. B* 116, 10165–10175.
- (55) Viet, M. H., Ngo, S. T., Lam, N. S., and Li, M. S. (2011) Inhibition of aggregation of amyloid peptides by beta-sheet breaker peptides and their binding affinity. *J. Phys. Chem. B* 115, 7433–7446.
- (56) Nguyen, T. T., Mai, B. K., and Li, M. S. (2011) Study of Tamiflu sensitivity to variants of A/H5N1 virus using different force fields. *J. Chem. Inf. Model.* 51, 2266–2276.
- (57) McQuarrie, D. A. *Statistical Thermodynamics*; HarperCollins: New York, 1973.
- (58) Miller, B. R., McGee, T. D., Swails, J. M., Homeyer, N., Gohlke, H., and Roitberg, A. E. (2012) MMPBSA.py: An Efficient Program for End-State Free Energy Calculations. *J. Chem. Theory Comput.* 8, 3314–3321.
- (59) Hawkins, G. D., Cramer, C. J., and Truhlar, D. G. (1996) Parametrized models of aqueous free energies of solvation based on pairwise descreening of solute atomic charges from a dielectric medium. *J. Phys. Chem.* 100, 19824–19839.
- (60) Hawkins, G. D., Cramer, C. J., and Truhlar, D. G. (1995) PAIRWISE SOLUTE DESCREENING OF SOLUTE CHARGES FROM A DIELECTRIC MEDIUM. *Chem. Phys. Lett.* 246, 122–129.
- (61) Weiser, J., Shenkin, P. S., and Still, W. C. (1999) Approximate atomic surfaces from linear combinations of pairwise overlaps (LCPO). *J. Comput. Chem.* 20, 217–230.
- (62) Laskowski, R. A., and Swindells, M. B. (2011) LigPlot+: multiple ligand–protein interaction diagrams for drug discovery. *J. Chem. Inf. Model.* 51, 2778–2786.
- (63) Gray, G. M., Ma, N., Wagner, C. E., and van der Vaart, A. Molecular dynamics simulations and molecular flooding studies of the retinoid X-receptor ligand binding domain. *J. Mol. Model.* 2017, 23, DOI: [10.1007/s00894-017-3260-9](https://doi.org/10.1007/s00894-017-3260-9)

Supporting information for:

**Bexarotene does not clear amyloid beta plaques but delays fibril growth:
Molecular mechanisms**

Pham Dinh Quoc Huy,^{†,‡,¶} Nguyen Quoc Thai,^{§,||,¶} Zuzana Bednarikova,[⊥] Le Huu Phuc,^{#,¶} Huynh Quang Linh,^{||} Zuzana Gazova,^{*,⊥} and Mai Suan Li^{*,†}

Institute of Physics, Polish Academy of Sciences, Al. Lotnikow 32/46, 02-668 Warsaw, Poland,

Institute for Computational Science and Technology, Quang Trung Software City, Tan Chanh Hiep Ward, District 12, Ho Chi Minh City, Vietnam, Contribution equally to the work, Division of Theoretical Physics, Dong Thap University, 783 Pham Huu Lau Str., Ward 6, Cao Lanh City, Dong Thap, Vietnam, Biomedical Engineering Department, University of Technology – VNU HCM 268 Ly Thuong Kiet Str., Distr. 10, Ho Chi Minh City, Vietnam, Department of Biophysics

Institute of Experimental Physics, Slovak Academy of Sciences, Watsonova 47, 040 01 Kosice, Slovakia, and Department of Theoretical Physics, University of Natural Sciences, VNU, Ho Chi Minh City, 227 Nguyen Van Cu, Dist. 5, Vietnam

E-mail: gazova@saske.sk; masli@ifpan.edu.pl

* To whom correspondence should be addressed

† Institute of Physics, Polish Academy of Sciences

‡ Institute for Computational Science and Technology, HCM city

¶ Contribution equally to the work

§ Division of Theoretical Physics, Dong Thap University

|| Biomedical Engineering Department, University of Technology - VNU HCM

⊥ Department of Biophysics Institute of Experimental Physics, Slovak Academy of Sciences

Department of Theoretical Physics, University of Natural Sciences - VNU HCM

Table S1: Binding free energy of bexarotene to $5\text{A}\beta_{17-42}$. Results were obtained using snapshots collected in equilibrium in 4 trajectories and MM-PBSA method.

Traj	ΔE_{vdw}	ΔE_{ele}	ΔG_{PB}	ΔG_{sur}	$-T\Delta S$	ΔG_{bind}
1	-30.2	-10.2	24.3	-3.2	18.7	-0.6
2	-33.9	-1.9	16.3	-3.8	16.5	-6.9
3	-35.7	-6.4	25.8	-3.6	19.2	-0.7
4	-22.0	-10.5	25.1	-2.8	15.4	+5.3
Average	-30.5 ± 6.1	-7.3 ± 4.0	22.9 ± 4.4	3.4 ± 0.4	17.5 ± 1.8	-0.7 ± 5.0

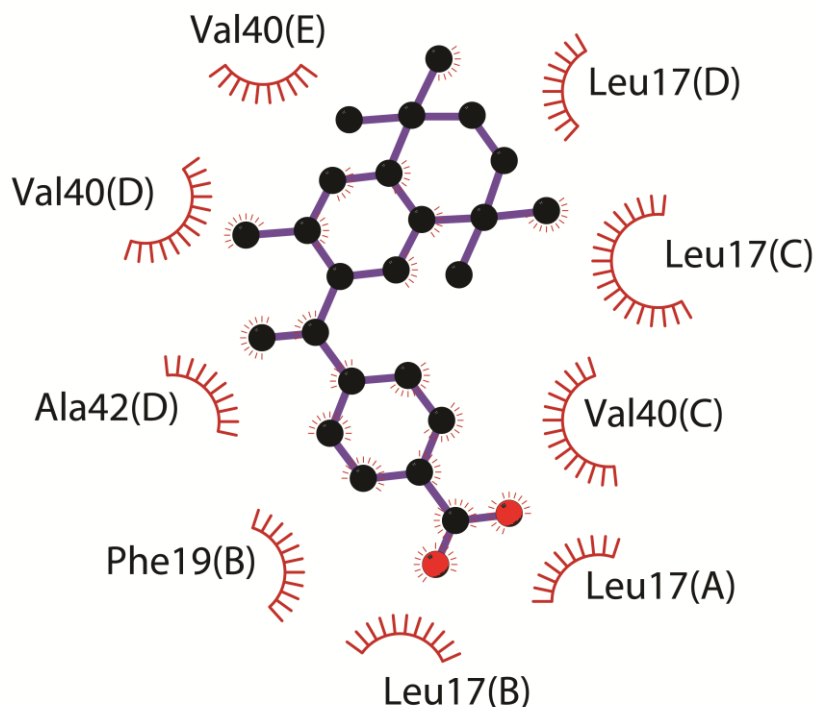


Figure S1: There is no HBs but Bexarotene forms 9 non-bonded contacts (represented by an arc with spokes radiating towards the ligand atoms they contact) with $5\text{A}\beta_{17-42}$. Capital letters in refer to the chains of fibril. The plot was prepared using LigPlot++ version 1.44.

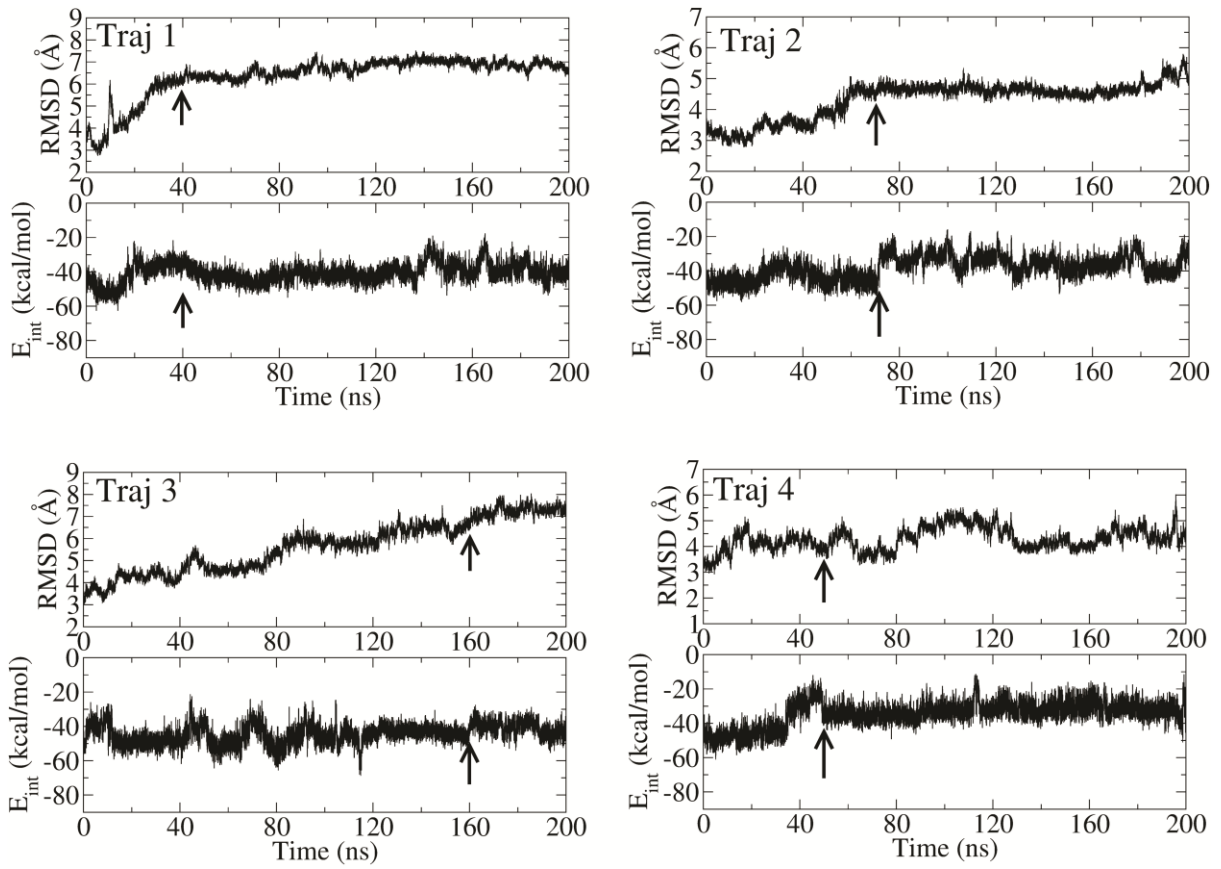


Figure S2: Time dependence of RMSD and the interaction energy (van der Waals and electrostatic) of $5\text{A}\beta_{17-42} + \text{bexarotene}$. The arrow indicates time when the complex reaches equilibrium.

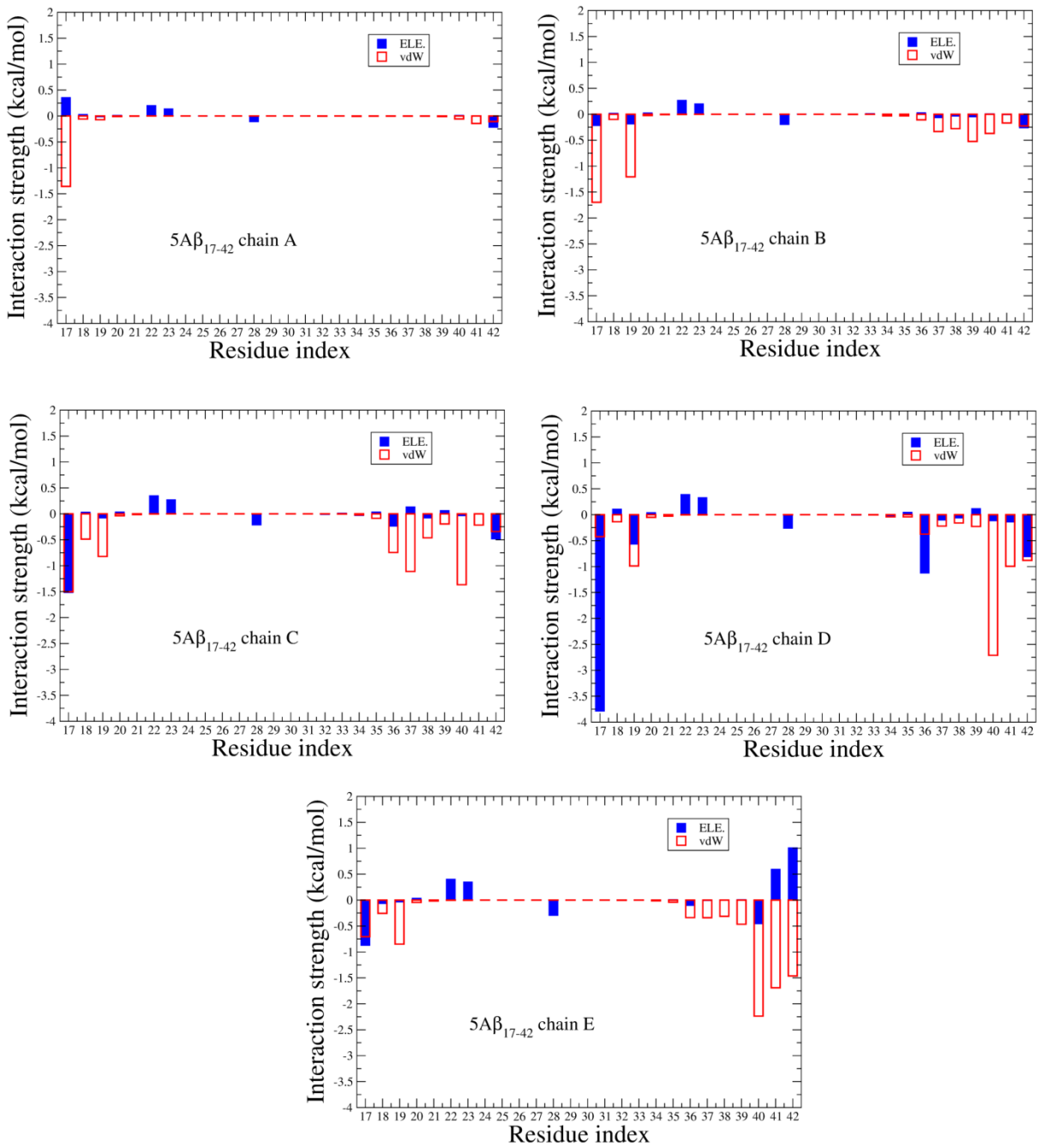


Figure S3. Per-residue distributions of the electrostatic and vdW interactions of $5\text{A}\beta_{17-42}$ fibril with bexarotene. Results were obtained at equilibrium and averaged over 4 MD runs.

Binding of bexarotene to 12A β ₁₁₋₄₂ (2MXU) fibril

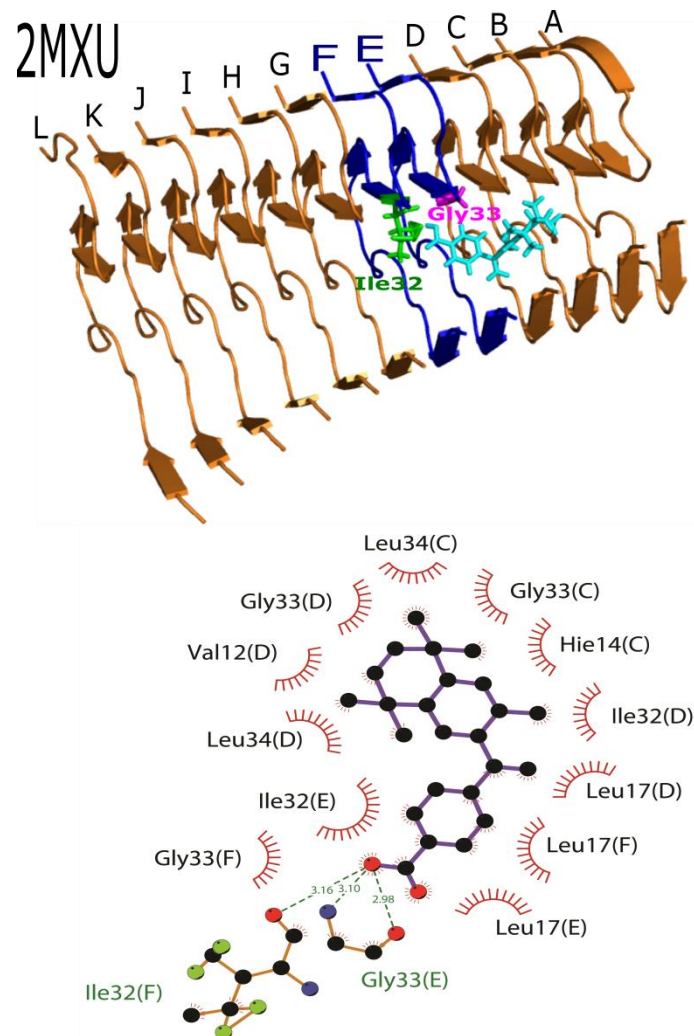


Figure S4. (A) Structure of 12A β ₁₁₋₄₂ + bexarotene complex in the best docking mode. 12 chains are referred to as A-L. Chains E and F are highlighted in blue because they participate in the HB network. (B) HB (dashed green line) and non-bonded contact (arc with spoke) networks in the lowest binding energy state. There are 3 HBs, formed by bexarotene with Gly33 from chain E and Ile32 from chain F, and 12 non-bonded contacts.

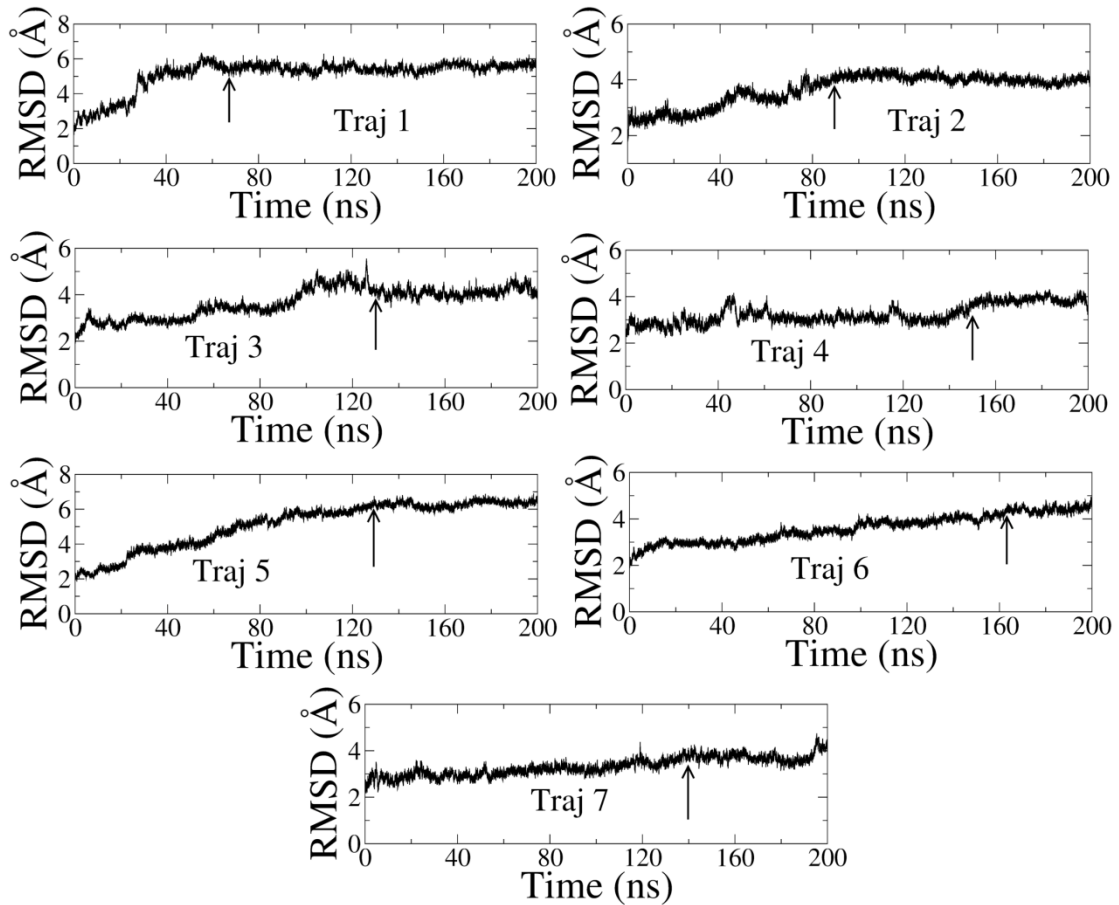


Figure S5: Time dependence of RMSD and the interaction energy (van der Waals and electrostatic) of $12\text{A}\beta_{11-42} + \text{bexarotene}$. The arrow indicates time when the complex reaches equilibrium.

Table S2: Binding free energy (kcal/mol) of bexarotene to $12\text{A}\beta_{11-42}$ (2MXU). Results were obtained using the MM-PBSA method and snapshots collected at equilibrium in 7 MD runs.

Traj	ΔE_{vdw}	ΔE_{ele}	ΔG_{PB}	ΔG_{Sur}	$-T\Delta S$	ΔG_{bind}
1	-44.9 ± 2.7	-6.0 ± 2.8	23.8 ± 3.3	-4.4 ± 0.1	15.0 ± 5.5	-16.5 ± 6.3
2	-47.4 ± 2.7	-2.5 ± 2.5	22.8 ± 3.9	-4.5 ± 0.1	20.6 ± 2.2	-11.0 ± 3.7
3	-33.8 ± 2.3	-1.3 ± 1.8	15.5 ± 2.7	-3.6 ± 0.1	16.9 ± 2.3	-6.3 ± 3.4
4	-51.2 ± 3.2	-4.6 ± 4.8	28.2 ± 4.8	-4.7 ± 0.1	16.1 ± 2.2	-16.2 ± 4.3
5	-37.7 ± 3.1	-4.5 ± 5.3	18.5 ± 4.2	-4.4 ± 0.1	14.3 ± 3.7	-13.8 ± 5.1
6	-48.4 ± 2.4	-4.1 ± 2.2	25.6 ± 3.5	-4.3 ± 0.1	14.6 ± 4.2	-16.6 ± 5.2
7	-43.1 ± 3.7	0.3 ± 1.7	15.6 ± 2.3	-4.2 ± 0.1	14.4 ± 5.1	-16.9 ± 5.9
Average	-43.8 ± 6.1	-3.2 ± 2.2	21.4 ± 4.9	-4.3 ± 0.3	16.0 ± 2.2	-13.9 ± 3.9

Binding of bexarotene to 10A β ₁₁₋₄₂ (5KK3) fibril

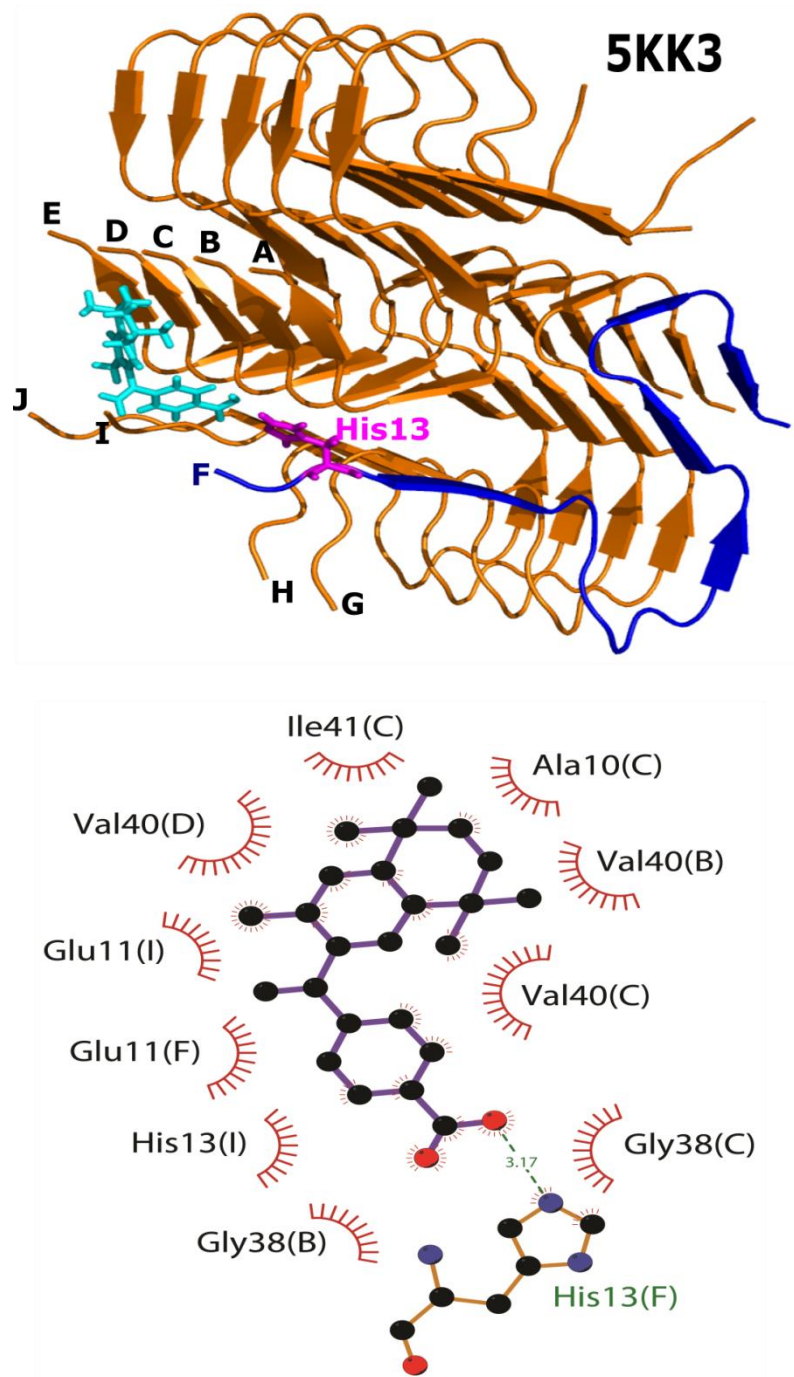


Figure S6. (A) Structure of 10A β ₁₁₋₄₂ + bexarotene complex in the best docking mode. Ten chains are denoted as A-J. Chain F is highlighted in blue as it has HB with bexarotene. (B) HBs and non-bonded contacts networks in the lowest binding energy state. A HB occurs between bexarotene and His13 from chain F.

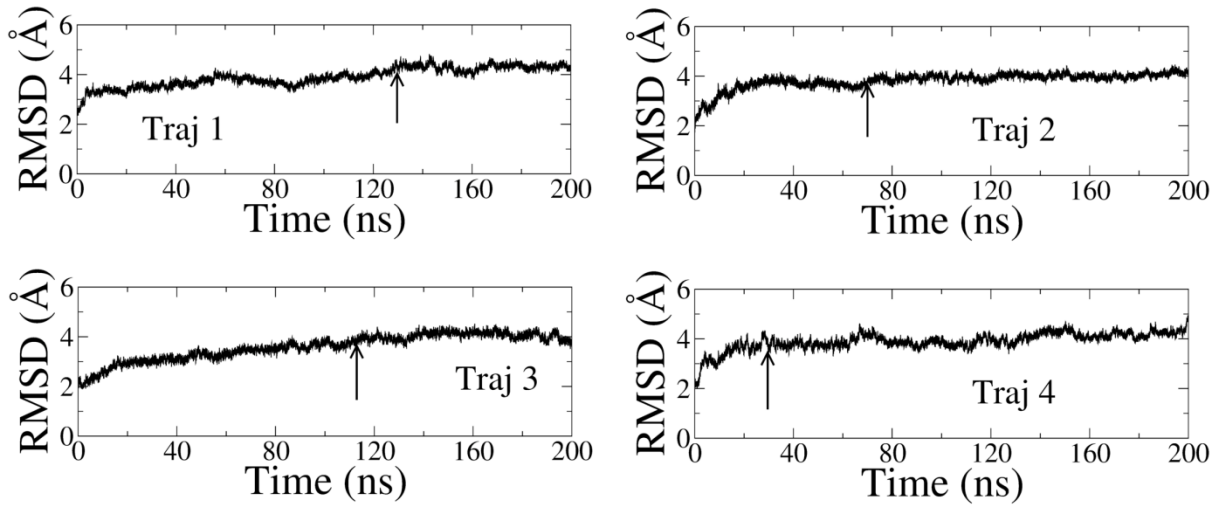


Figure S7: Time dependence of RMSD and the interaction energy (van der Waals and electrostatic) of $10\text{A}\beta_{11-42} + \text{bexarotene}$. The arrow indicates time when the complex reaches equilibrium.

Table S3: Binding free energy (kcal/mol) of bexarotene to $10\text{A}\beta_{11-42}$ (5KK3). Results were obtained using the MM-PBSA method and snapshots collected at equilibrium in 4 MD runs.

Traj	ΔE_{vdW}	ΔE_{ele}	ΔG_{PB}	ΔG_{Sur}	$-T\Delta S$	ΔG_{bind}
1	-25.1 ± 2.8	-8.7 ± 7.1	20.6 ± 7.1	-2.9 ± 0.1	16.5 ± 1.1	0.3 ± 2.8
2	-29.5 ± 6.2	-3.3 ± 4.0	15.0 ± 4.8	-3.1 ± 0.4	16.3 ± 1.5	-4.5 ± 4.8
3	-19.7 ± 3.6	-7.1 ± 5.1	15.7 ± 5.2	-2.4 ± 0.3	16.1 ± 5.6	2.6 ± 6.2
4	-21.2 ± 3.6	-3.1 ± 6.4	10.6 ± 5.8	-2.5 ± 0.3	14.7 ± 2.6	-1.6 ± 3.7
Average	-23.9 ± 4.4	-5.6 ± 2.8	15.5 ± 4.1	-2.7 ± 0.3	15.9 ± 0.9	0.8 ± 3.0

Binding of bexarotene to 6A β ₁₋₄₂ (2NAO) fibril

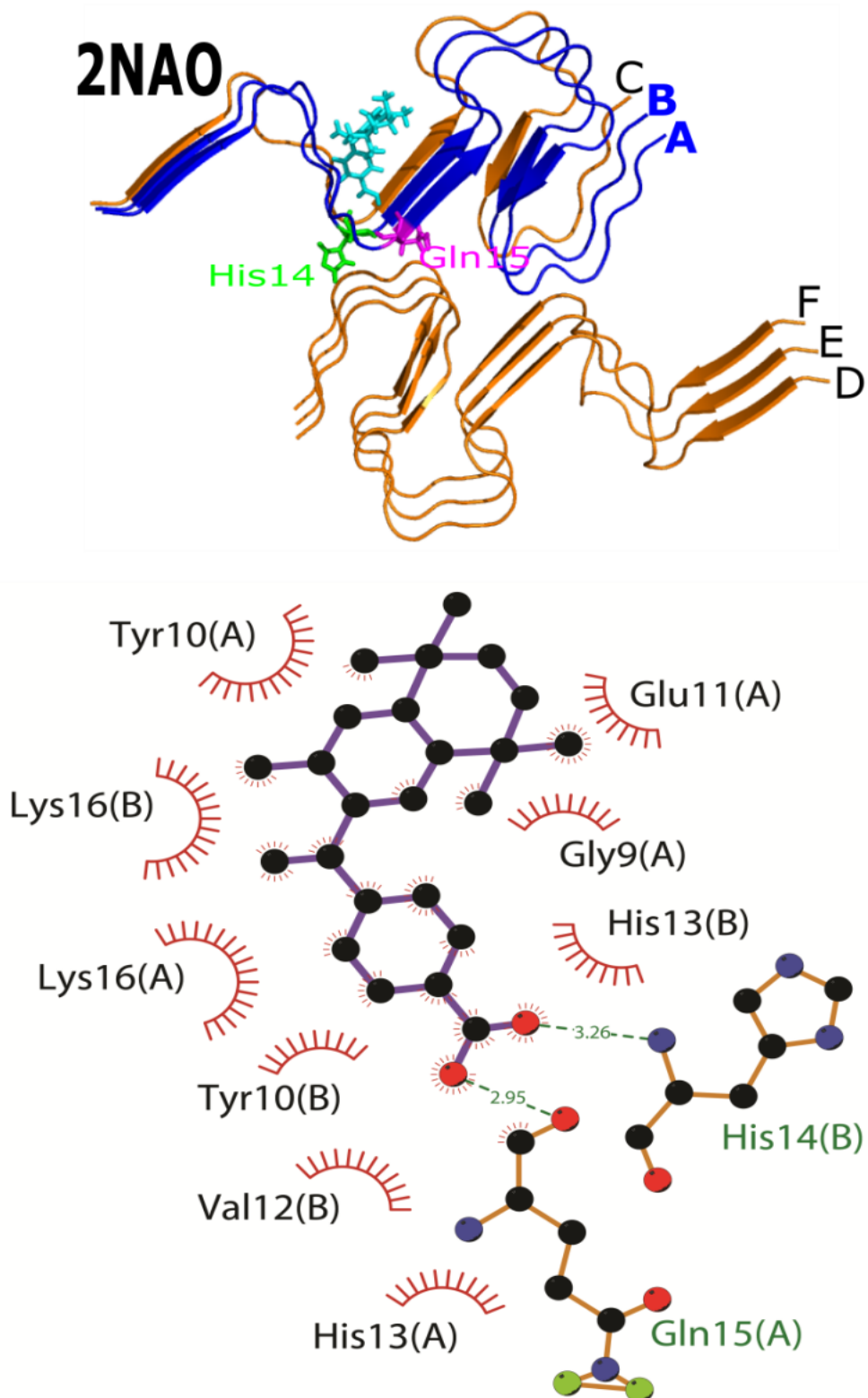


Figure S8. (A) Structure of 6A β ₁₋₄₂+bexarotene complex in the best docking mode. Six chains are referred to as A-F. (B) HBs and non-bonded contacts networks in the lowest binding energy state. Two HBs occur between bexarotene and Gln15 (chain A) and His14 (chain B).

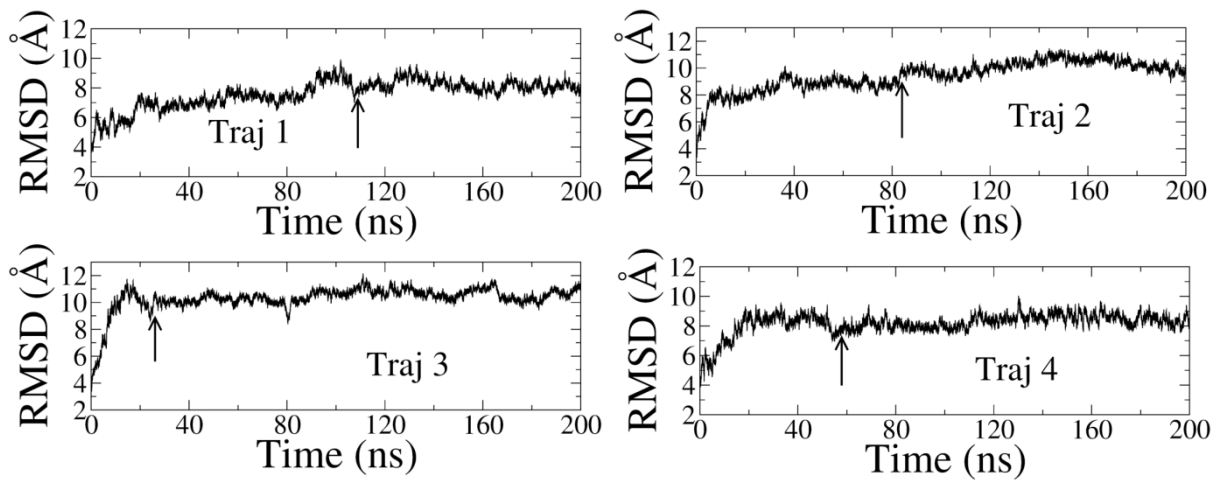


Figure S9: Time dependence of RMSD and the interaction energy (van der Waals and electrostatic) of $6\text{A}\beta_{1-42} + \text{bexarotene}$. The arrow indicates time when the complex reaches equilibrium.

Table S4: Binding free energy (kcal/mol) of bexarotene to $6\text{A}\beta_{1-42}$ (2NAO). Results were obtained using the MM-PBSA method and snapshots collected at equilibrium in 4 MD trajectories.

Traj	ΔE_{vdW}	ΔE_{ele}	ΔG_{PB}	ΔG_{Sur}	$-\text{T}\Delta S$	ΔG_{bind}
1	-20.6 ± 7.1	-7.2 ± 8.3	18.8 ± 11.0	-2.4 ± 0.5	18.2 ± 10.7	6.7 ± 11.4
2	-34.3 ± 2.2	-8.7 ± 2.8	24.4 ± 3.4	-3.1 ± 0.1	18.1 ± 4.9	-3.6 ± 5.9
3	-20.6 ± 7.7	-4.6 ± 5.2	14.1 ± 6.5	-2.5 ± 0.7	16.8 ± 2.4	3.0 ± 5.9
4	-42.6 ± 3.7	-4.6 ± 5.3	26.8 ± 4.9	-4.2 ± 0.1	17.6 ± 4.1	-7.0 ± 5.6
Average	-29.5 ± 10.8	-6.3 ± 2.0	21.0 ± 5.7	-3.1 ± 0.8	17.7 ± 0.6	-0.2 ± 6.2

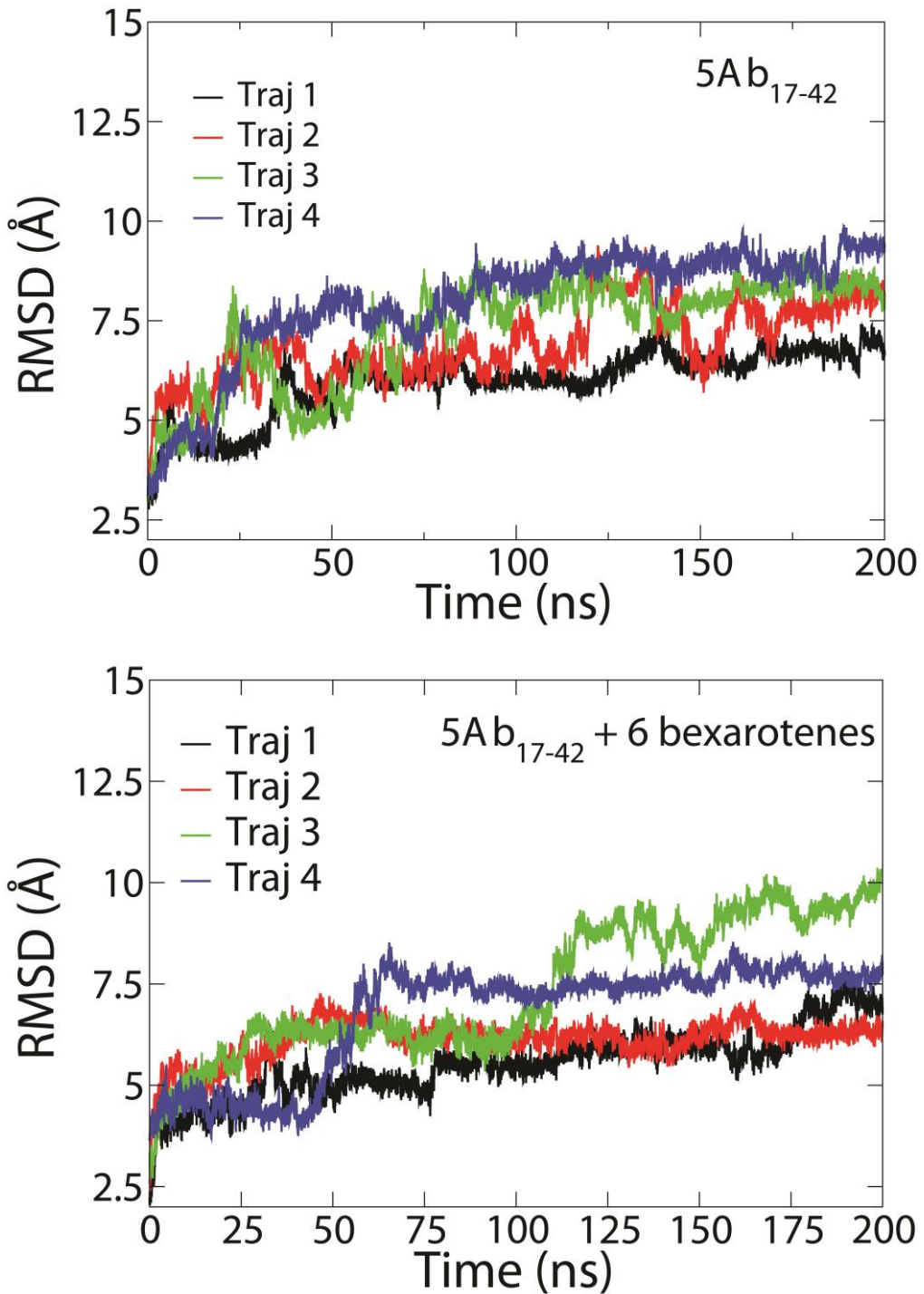


Figure S10: Time dependence of RMSD for $5\text{A}\beta_{17-42}$ (upper panel), where 4 independent MD runs started from the PDB structure but with different random seed numbers. The lower panel refers to the $5\text{A}\beta_{17-42} + 6$ bexarotenes complex. Here MD trajectories 1, 2 and 3 started from initial configurations with 6 bexarotene molecules randomly placed around the PDB structure. In the starting configuration of trajectory 4 five bexarotenes reside at the best docking positions and the position of sixth bexarotene was selected at random.

Binding of bexarotene to monomer

To estimate the binding free energy of bexarotene to monomer we have used 9 representative structures obtained by the molecular dynamics simulation.^{S1}

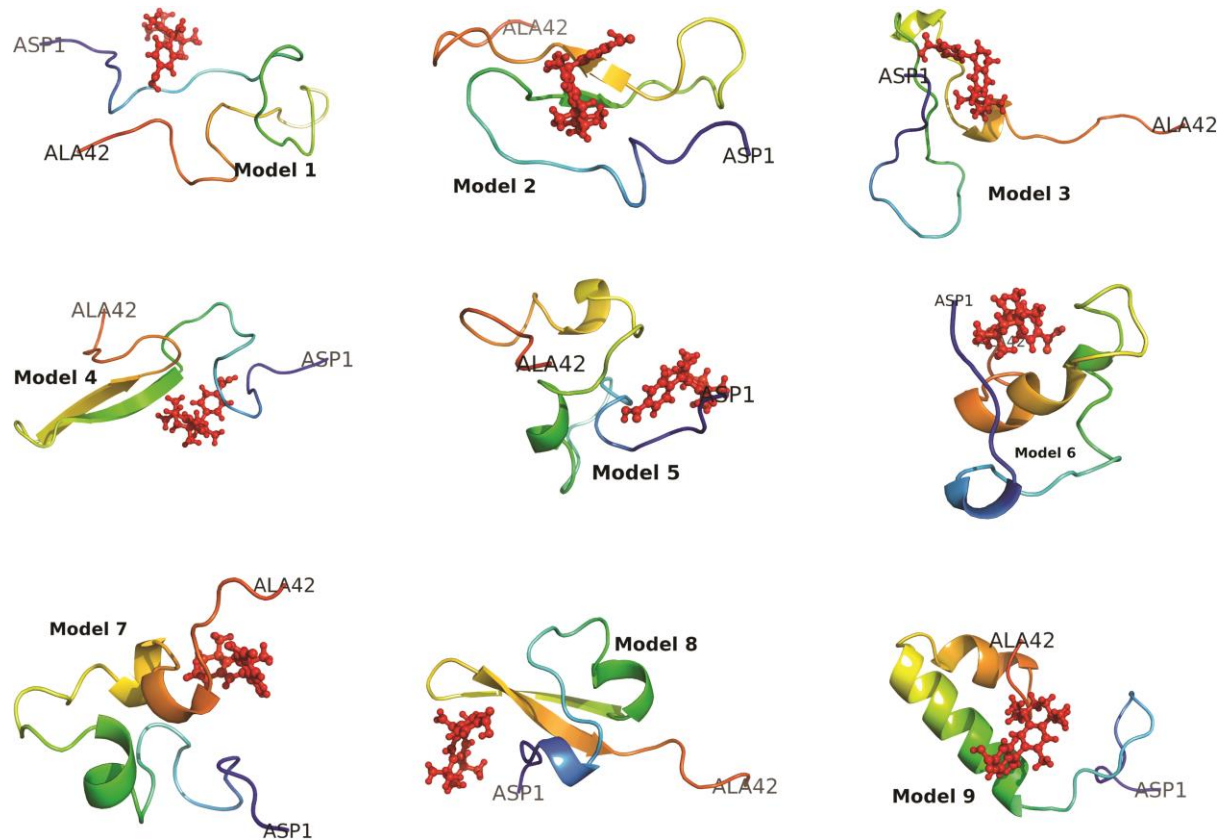


Figure S11: 9 models of $A\beta_{1-42}$ monomer in the best docking mode with bexarotene (red). Taken from Yang and Teplow.^{S1}

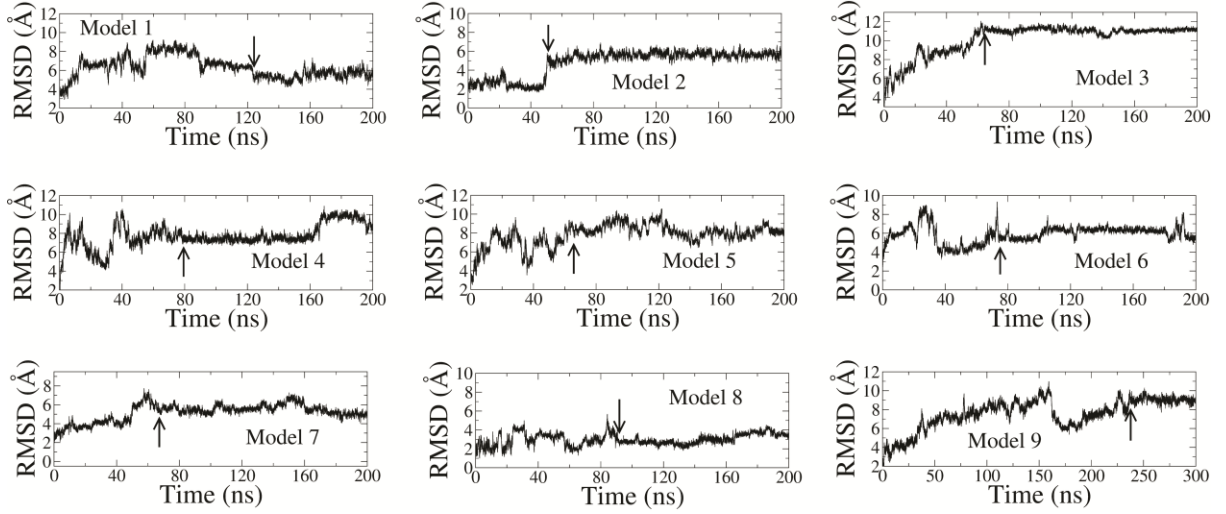


Figure S12: Time dependence of RMSD of $A\beta_{1-42}$ + bexarotene complexes during the 200 ns MD simulation. The arrow refers to time when RMSD saturates or the system reaches equilibrium.

Table S5: Binding free energy (kcal/mol) of bexarotene to monomer $A\beta_{1-42}$. Results were obtained by the MM-PBSA method.

Model	ΔE_{vdW}	ΔE_{ele}	ΔG_{sur}	ΔG_{PB}	$-T\Delta S$	ΔG_{bind}
1	-31.2	-14.6	-3.3	26.6	15.2	-7.4
2	-37.0	-3.9	-3.7	20.5	18.9	-5.1
3	-22.6	-3.8	-2.7	14.1	16.7	1.7
4	-21.0	-2.9	-2.5	10.1	17.5	1.2
5	-29.6	-9.4	-3.4	24.6	19.1	1.3
6	-33.8	-13.1	-3.1	22.9	18.4	-8.7
7	-24.7	-8.1	-2.9	17.6	15.5	-2.7
8	-16.7	-7.5	-2.1	14.7	16.3	4.7
9	-21.8	-6.0	-2.6	14.3	15.1	-1.0
Average	-26.5	-7.7	-2.9	18.4	17.0	-1.8

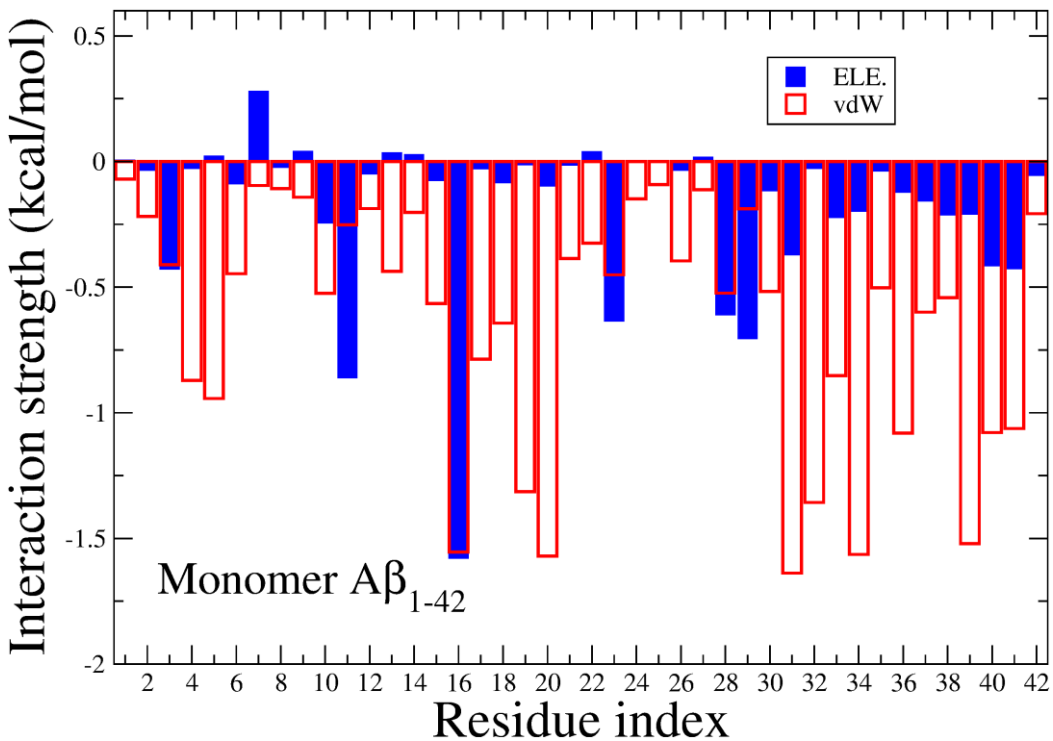


Figure S13. Per-residue distributions of the electrostatic and vDW interactions of $\text{A}\beta_{1-42}$ monomer with bexarotene. Results were obtained at equilibrium and averaged over 9 MD runs.

Binding of bexarotene to dimer

To compute the binding free energy of bexarotene to $A\beta_{1-42}$ dimer we used the structure from Zhang *et al.*^{S2}

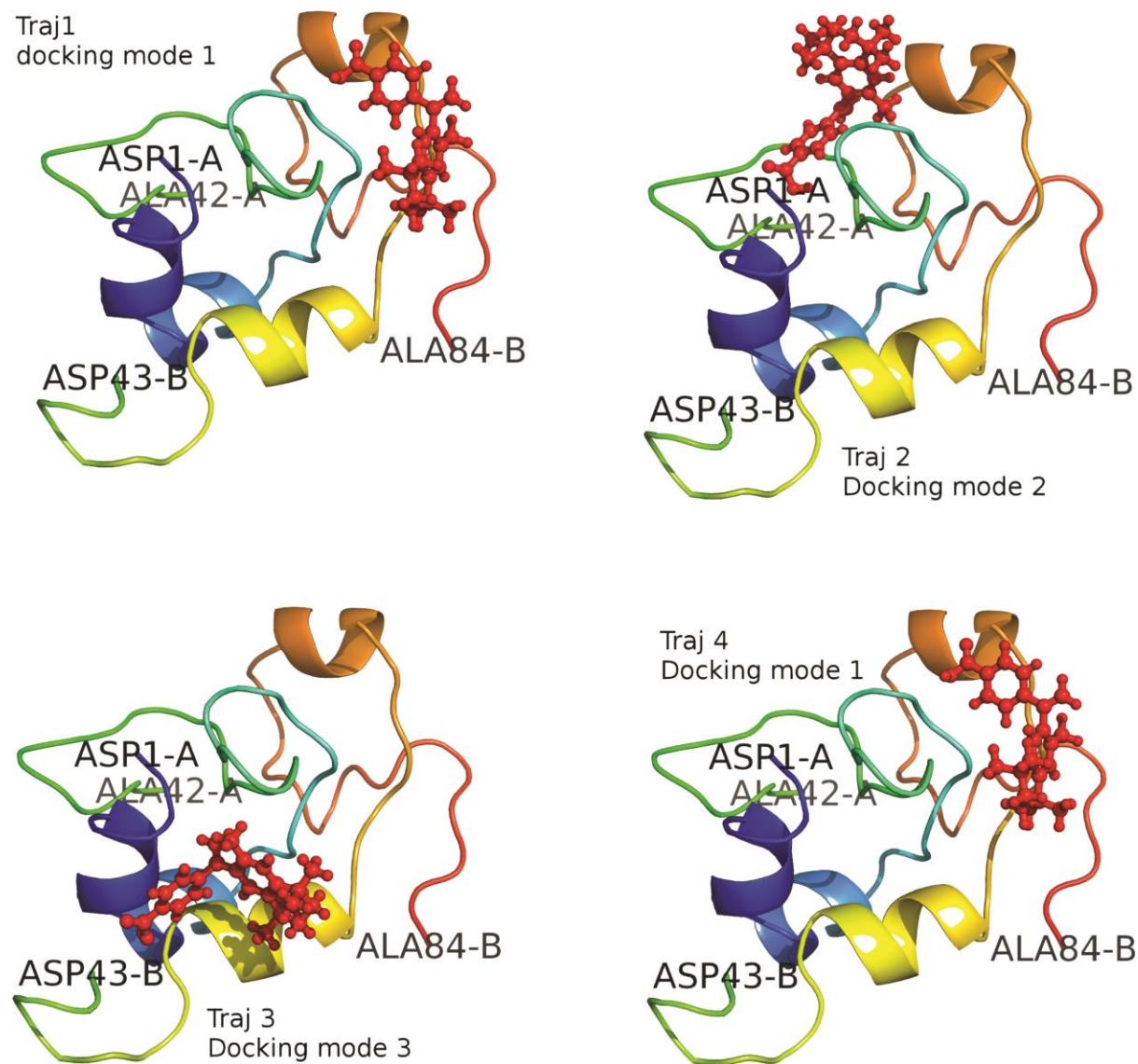


Figure S14: Starting configurations for $A\beta_{1-42}$ dimer with bexarotene. Trajectories 1 and 4 have the same starting structure with bexarotene in the docking mode 1 but with different random seed numbers, while trajectories 2 and 3 correspond to the second and third binding modes, respectively.

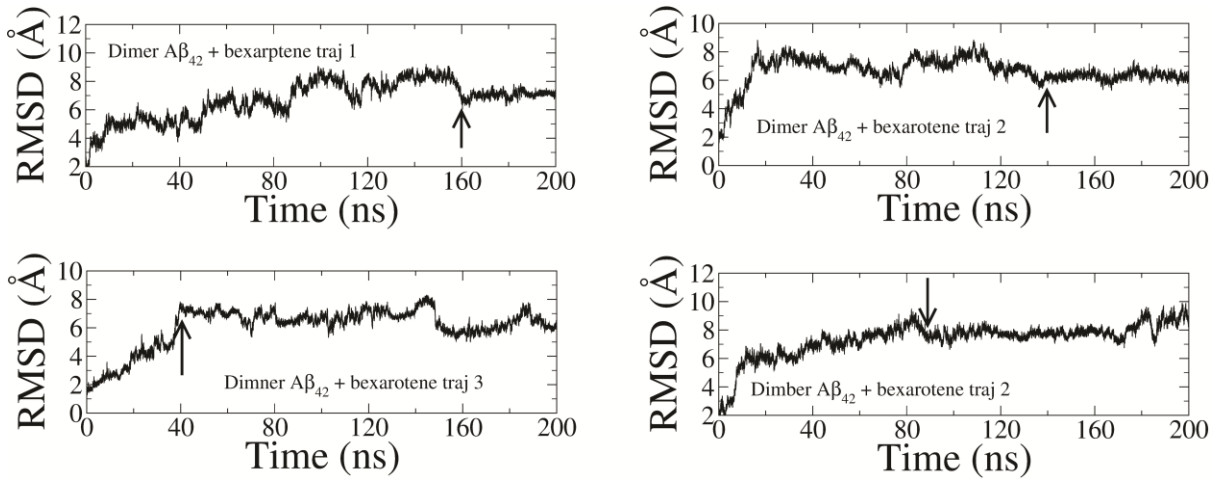


Figure S15: Time dependence of RMSD of the dimer + bexarotene complex. The arrows refer to time when RMSD saturates fluctuating around its equilibrium value.

Table S6: Binding free energy (kcal/mol) of bexarotene to $A\beta_{1-42}$ dimer.

Traj	ΔE_{vdW}	ΔE_{ele}	ΔG_{sur}	ΔG_{PB}	$-T\Delta S$	ΔG_{bind}
1	-27.5	-12.5	-3.1	21.0	17.8	-4.3
2	-8.0	-1.2	-1.1	4.1	11.2	5.0
3	-20.1	-1.9	-2.5	11.0	14.3	0.9
4	-18.3	-14.7	-1.8	21.7	14.0	0.9
Average	-18.5	-7.6	-2.1	14.5	14.3	0.6

REMD simulation of A β ₁₋₄₂ + 10 bexarotenes

The 200 ns REMD simulation was conducted with 64 replicas in the temperature interval [290,492.91K] including

290, 292.58, 295.18, 297.79, **300.43**, 303.08, 305.75, 308.44, 311.15, 313.87, 316.62, 319.38, 322.16, 324.97, 327.79, 330.63, 333.49, 336.37, 339.27, 342.19, 345.13, 348.08, 351.06, 354.06, 357.09, 360.13, 363.19, 366.28, 369.38, 372.51, 375.66, 378.82, 382.01, 385.23, 388.47, 391.73, 395.01, 398.32, 401.65, 405.01, 408.45, 411.84, 415.27, 418.71, 422.19, 425.68, 429.20, 432.74, 436.31, 439.89, 443.51, 447.15, 450.82, 454.51, 458.23, 461.98, 465.75, 469.55, 473.38, 477.23, 481.11, 485.02, 488.95, 492.91.

The mean acceptance rate was 23.52%. Data obtained at $T=300.43$ were used for data analysis.

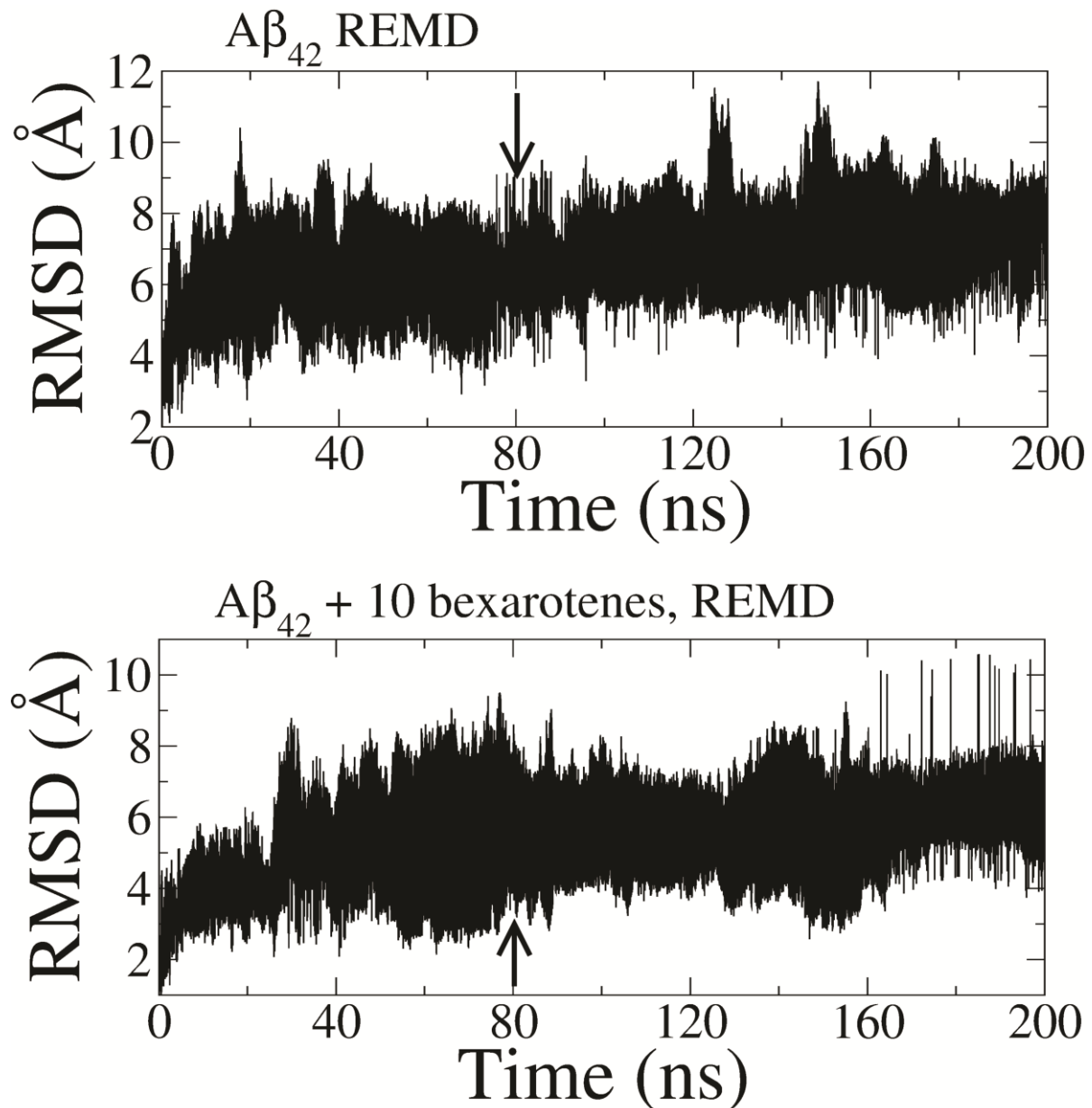


Figure S16: Time dependence of RMSD of $A\beta_{1-42}$ and $A\beta_{1-42} + 10$ bexarotenes. The arrow refers to time when the system reaches equilibrium which corresponds to saturation of RMSD. Results were obtained by the REMD simulation.

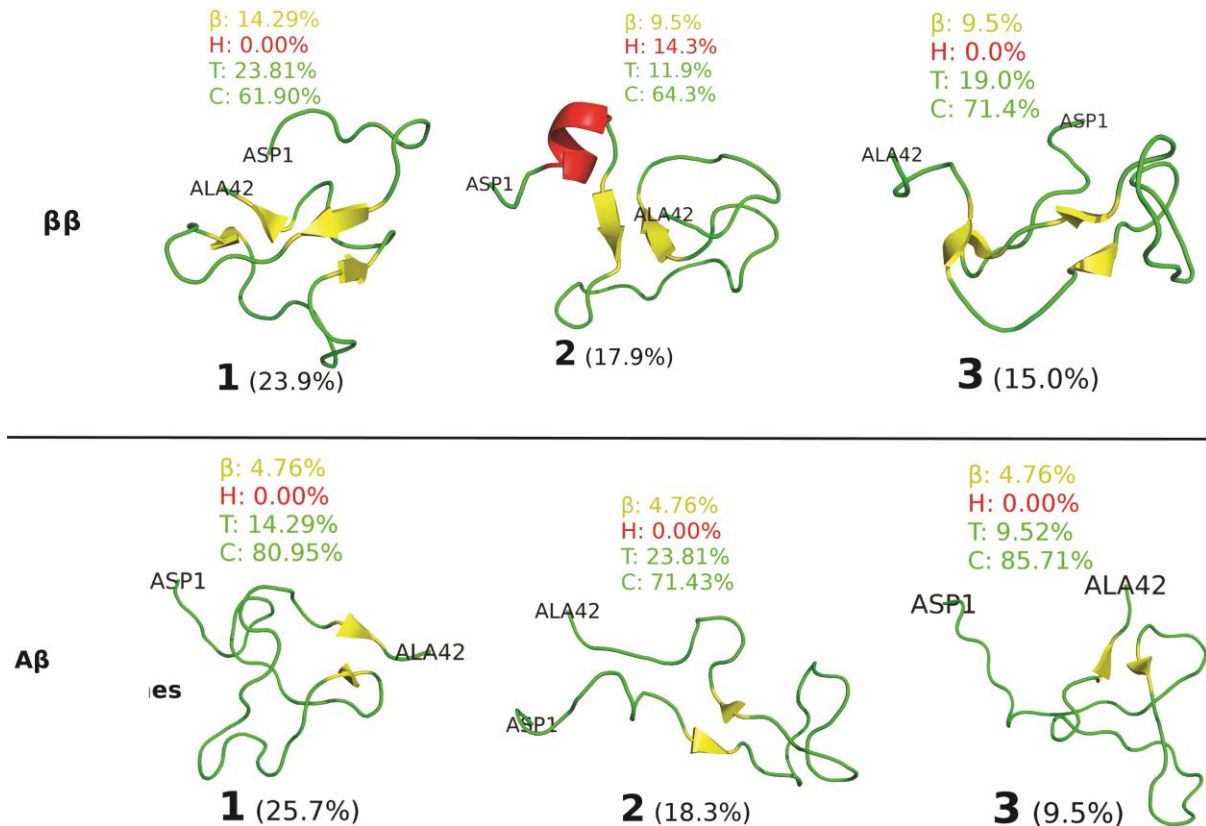


Figure S17: Representative structures of three most populated structures of $\text{A}\beta_{1-42}$ and $\text{A}\beta_{1-42} + 10$ bexarotenes. For $\text{A}\beta_{42}$ the populations (shown in brackets) of clusters 1, 2 and 3 are 23.9, 17.9, and 15.0%. For $\text{A}\beta_{1-42} + 10$ bexarotenes the corresponding populations are 25.7, 18.3 and 9.5%. The β , helix (H), turn (T) and coil (C) contents are also shown. Results were obtained in the REMD simulation.

Movie

Movie 1: Evolution of $\text{A}\beta_{1-42} + 10$ bexarotenes conformations during 200 ns of REMD simulation at $T=300.43$ K.

Movie 2: Evolution of $\text{A}\beta_{1-42} + 10$ bexarotenes conformations during 1000 ns of conventional simulation at $T=300.43$ K.

References

- (S1) Yang, M.; Teplow, D. B. *J. Mol. Biol.* **2008**, *384*, 450-464.
- (S2) Zhang, Y.; Hashemi, M.; Lv, Z.; Lyubchenko, Y. L. *Nanoscale* **2016**, *8*, 18928-18937.